INTERNATIONAL JOURNAL OF ADVANCED ENGINEERING AND BUSINESS SCIENCES (IJAEBS)
Journal homepage: https://ijaebs.journals.ekb.eg

Performance of High Strength Steel Fibre Reinforced Concrete Deep Beams

F.B.A. Beshara[1], Ahmed. A. Mahmoud[2] and A. A. El-Barbary[3]

1 Associate Professor, Department of civil engineering, faculty of engineering (Shoubra), Benha University,108 Shoubra St., Shoubra, Cairo, Egypt

2 Professor of Reinforced Concrete Structures, Department of civil engineering, faculty of engineering (Shoubra), Benha University,108 Shoubra St., Shoubra, Cairo, Egypt

3 Assistance Professor of Structural Engineering, Delta Higher Institute for Engineering and Technology, El Mansoura, Egypt

Received: 24-09-2022 **Accepted:** 27-11-2022 **Published**: 01-02-2023

ABSTRACT

This paper presents the results of an experimental program and a nonlinear numerical investigation on the behavior of high strength steel fibre reinforced concrete deep beams under monotonic static loads. Seventeen simply-supported deep beams are tested and analyzed**.** The mean compressive strength of concrete is 60 MPa. The specimens are divided into five groups with different structural parameters. The studied parameters are: (1) steel fibre volume fractions, (2) fibres aspect ratios, (3) shear span-to-depth ratios, (4) horizontal web reinforcement and (5) vertical web reinforcement ratios. The measured testing results are used to study the influence of steel fibres on the structural response such as: (1) the first diagonal cracking load, (2) failure load, (3) load-deflection curves, (4) load-steel strain relationships, (5) failure modes, and (6) crack propagation patterns. The testing results indicated that the load carrying capacity at different levels, and displacement ductility increased considerably with the increase of fibre volume and/or fibre aspect ratio. Also, inclusion of steel fibres delays the crack propagation process and reduces the deflection and crack width. Also, the results showed that the measured concrete strain profiles at critical sections are nonlinear. In this study, the tested beams were modeled using ANSYS nonlinear finite element program which was modified to include the fibres enhancement on the stress-strain relations and failure surface. The finite element predictions of the structural response show good agreement with the observed experimental behavior.

Keywords: Shear strength; high strength concrete; deep beams; steel fibres; nonlinear finite element method; and ANSYS program.

1 INTRODUCTION

Deep beams are structural elements having a depth comparable to the span length. The CIRIA Guide [1] applies to beams having an effective span to total depth ratio Le/h of less than 2 for single-span beams and less than 2.5 for continuous beams. Also, Egyptian Code ECP [2] defines the deep beam as the beam having an effective span to depth ratio Le/h of less than 1.25 for single-span beams and less than 2.5 for continuous beams. According to American code ACI 318-11 [3] deep beams are the members with ratio of clear span to overall height Ln to h less than 4, or regions of beams with concentrated loads within a distance 2h from the support that are loaded on one face and supported on the opposite face so that compression struts can develop between the loads and supports.

The use of deep beams is widespread in modern structures; it has useful applications in tall buildings as transfer girders, in bridges as bent caps and in foundations as pile caps and foundation walls. There are extensive experimental and analytical investigations to study the behavior and failure mechanisms of the reinforced concrete deep beams [4-9]. The main studied parameters in the research work were the effect of shear span-to-depth ratio, concrete strength, and web reinforcement ratio on the structural response.

Many reports published over the past four decades [10-12] confirm that the use of randomly oriented discrete short steel fibres is effective in showing the mechanical properties of brittle concrete matrix. Also, it increases the member stiffness and ductility in flexural and shear. Steel fibres offer a good crack width control mechanics and slow the rate of propagation of cracking process. Steel fibers have hooked ends or have a thin wavy shape or thick corrugated shape to improve resistance to pullout from cement –based matrix and so having strong bonding with concrete which are commonly used. In this study two types of steel fibers are used from the products of Zamil steel company Ltd. The first type is thick corrugated shape with aspect ratio (L_f / Φ_f) = 60 with different volume (V_f = 0.5% and 1%), and the second type is thin wavy with aspect ratio (L_f / Φ_f) = 80 with different volume (V_f = 0.5% and 1%) as will be mentioned later.

In the literature, several investigations [13-16] are reported for the behavior of normal strength fibre reinforced concrete deep beams where the roles of fibre volume, fibre aspect ratio and fibre types were studied. Also, some finite element models and studies [17-19] are documented for predicting the response of deep beams. The use of steel fibres is proved to be effective in overcoming the brittleness of high strength concrete. However, very few studies are performed on high strength steel fibre reinforced concrete deep beams [20-22 and 32-40].

In the present work, the results of a comprehensive experimental program [32-34] and analytical studies [35-36] are reported to study the influence of steel fibres inclusion on the behavior of high strength reinforced fibre concrete deep beams. Main attention is directed to: (1) shear carrying

capacity, (2) load-deflection curves, (3) load-steel strain relationships, (4) concrete strain distribution profiles, (5) failure modes, and (6) crack propagation under monotonic static loading. Also, the nonlinear finite element analysis program; ANSYS, was used to predict the structural response of the tested deep beams. The concrete model in ANSYS program was modified to account for the effect of fibre inclusion in tension and compression.

2 EXPERIMENTAL PROGRAM

2.1 Test specimens and materials

The test specimens included seventeen simply-supported deep beams with constant cross section of total depth 500 mm and width 120 mm. The overall dimensions of the typical specimens are shown in Fig. 1 and Table 1. The provided flexural and shear reinforcement were chosen to satisfy the requirements of the Egyptian Code ECP [2]. The specimens were reinforced by two bottom steel bars of 18-mm diameter and two top steel bars of 10-mm diameter as secondary top reinforcement. The corresponding tension steel ratio is ρ_s = 0.90 %. The longitudinal reinforcement was high-tensile steel bars. The web reinforcement for all beams was mild steel bars 8-mm diameter as horizontal and vertical stirrups. The properties of steel bars were obtained from the results of the tension tests carried out for three samples of bars for each diameter. The proof stress for longitudinal bars was 438 MPa and the yield stress for web reinforcement was 299 MPa. For concrete, a trial mix design has been conducted using locally available materials. The mixes were designed to get characteristic compressive strength of standard cube as greater or equal 60 MPa at 28 days with water/cement ratio (W/C) 0.38.

According to the structural key parameters, the specimens were divided into five main groups as given in Table 1. For the first three groups A, B and C, the shear span-to-depth ratio *a/d* was 0.44, 0.81 and 1.0 respectively. The specimens of these three groups contain different fibres volume content V_f as 0.0%, 0.5% and 1.0%, and different fibres aspect ratio l_f/ϕ_f as 0, 60 and 80. For the specimens of other two groups H and V where *a/d* = 0.81, the fibre parameters were constant as V_f = 1% and l_f/ϕ_f = 80. The volumetric ratio of vertical web reinforcement ρ_v and horizontal web reinforcement ρ_h web steel for groups A, B and C was constant and equals 1.12%. For group H, the horizontal web reinforcement ratio ρ_h was 0.0, 0.84 and 1.68 with constant vertical stirrups ratio ρ_v =1.12%. For group V, the vertical web reinforcement ratio ρ_v was 0.0, 0.84 and 1.68 while the horizontal web reinforcement ratio was constant ρ_h =1.12%.

2.2 Testing procedure and instrumentation

The specimens are tested up to failure using a calibrated compression-testing machine of 5000 kN capacity and 0.10 kN accuracy. The testing machine consists of lower moving piston which moves on a spherical head covered by steel plate so, that the applied load is always passing through the center of the sphere. All beams are exposed to loading on two symmetrical points with the required shear span. The specimens are rested on two supports, one of them is roller and the other one is hinged. To prevent local failure due to bearing stresses at both points of loadings and supports, steel plates (500x 100 X 40 mm) are used. The load was measured through a pressure sensor that was fed-in addition to other test data-into a data acquisition system. The voltage excitations were read, transformed and stored as micro strains, forces, and displacements by means of a virtual instant computer program runs under (LABVIEW) software. Each beam was laterally stiffened by four wooden arms ended by rubber wheel to prevent the lateral movement (out of the beam plan) during loading as shown in Fig. 2. The loading process starts with a certain load interval (100 kN), then it was stopped to notice the cracks and to mark their development and its propagation. After reaching the first crack, the loading increments decreased to (50 kN) to follow the cracks propagation. All results were recorded automatically using the data logger. Electrical strain gauges were used to measure the strains in concrete surface, in the main longitudinal bottom steel, and in the vertical and the horizontal stirrups. The corresponding vertical deflection at the mid-span was measured using LVDT as shown in Fig. 3. The demic points were used to draw the surface concrete strain distribution along the beam depth. The distance between each couple of demic points were 100 mm.

3 Experimental Results

3.1 Observed behavior and failure modes

Specimen with bigger *a/d* has earlier appearance and rapid development of cracks. In almost all beams, the observed flexural crack appeared earlier than the diagonal shear cracks. The first flexural crack was vertical and appeared in the flexural sagging region (mid-span) at approximately between 30 % and 40 % of the failure load. Then, the first crack in the diagonal direction appears approximately between 50 % and 75 % of the failure load. The shear cracks extended towards both the support and the loading points; parallel to the strut connecting the points of loading and the points of supports. The inclination angles of the diagonal cracks are ranged between 45 and 65^{o}. Further increase in load resulted in the propagation and widening of the existing cracks; and simultaneously, new diagonal cracks developed more or less parallel to the existing ones. Some of these new cracks had originated vertically, but later become sloped in a diagonal direction. This change in slope is probably caused by

a movement upward of the neutral axis as the cracks progress upward with increasing load. This change in position of the neutral axis with increasing load was observed directly from the surface concrete strain. The influence of fibre content V_f and fibre aspect ratio l_f/ϕ_f is very sensitive; the increase of V_f or l_f/ϕ_f enhances the shear and tension resistances of concrete and plays an important role to bridge and arrest the cracks as shown in Fig. 4. This is the reason of delay of appearance of the first flexural and diagonal shear cracks for fibrous deep beams.

Table 2 summarized the observed failure modes for all tested beams. The observed failure modes for deep beams were namely: (1) shear-compression failure (S.C)**,** (2) diagonal-splitting failure (D.S) and (3) crushing of concrete strut (C.S). Figure 4 shows the various crack patterns and the different modes of failure. The first mode is shear-compression failure which is concerned with low *a/d* ratios such as beams A2 and A3; shown in Fig. 5-a this type of failure occurred in beam with high horizontal ρ_h and vertical ρ_v web reinforcement ratios such as beam H1. This mode of failure is brittle and accompanied with a loud explosive noise at failure.

The second mode of failure is diagonal splitting (D.S) which is less brittle (ductile) compared to the first one and is characterized by non-explosive sound. During the failure process, the failure load of fibrous beams was able to be degraded on the specimens despite wide cracks due to the post-cracking strength of steel fibres. Degradation of the load carrying capacity started with the pull-out or the rupture of fibres across the opened cracks as shown in Figs. 4 and 5. At impending failure, some crushing particles of the concrete were observed between the loading points and the tip of the major inclined crack. This mode is related to high values of each V_f, l_f/ϕ_f and *a/d* ratios, such as beams B2 and C1 as shown in Fig. 5-b. During the cracking development process under the increasing load, the concrete strut between the inclined cracks failed in compression. This mode of failure is brittle and sudden and can be classified as crushing of strut failure such as beam C2 and V3 as shown in Fig. 5-c.

3.2 Mid-span deflection and failure load

In the early stages of loading, the beams behaved in an elastic manner and the load-deflection relations were linear. After first diagonal cracking, the response is nonlinear and is characterized by a curvilinear manner. The measured load-deflection curves of the tested beams were grouped in order to study the effects of the testing variables. In Table 2, the experimental results are given for the measured: (1) first diagonal cracking load P_{crs}, (2) the failure load $P_{f\,EXP)}$, (3) the failure load $P_{f\,(EXP)}$ (4) the deflections at the yield level Δ_y and (5) the deflection at failure load Δ_f. The displacement ductility of each beam $\phi_{\Delta f}$, is also calculated as the ratio between the deflections at failure to the deflection at yield.

$$\phi_{\Delta f} = \Delta_f / \Delta_y \quad (1)$$

For different fibre volume ratios V_f = 0.0 %, 0.5 % and 1% (with constant fibre aspect ratio l_f/ϕ_f = 80), the measured loads-deflection till failure are drawn in Fig.6 for beams A0, A1, A3, C0, C1 and C2. Also, the effect of fibre aspect ratio l_f/ϕ_f = 0.0, 60 and 80 (with constant fibre volume V_f = 1.0 %,), on the measured load-deflection curves is plotted in Fig. 7 for A0, A2, A3, B0, B2 and B3. From the results of these figures and Table 2, it can be seen that the increase of fibre volume V_f or fibre aspect ratio l_f/ϕ_f leads to an increase in the failure load carrying capacity $P_{f(EXP)}$ as a result of the enhanced post-cracking strength of steel fibre reinforced concrete. Also, the increase of fibre aspect ratio increases the pull-out resistance of fibres. As V_f increased from 0.0 % to 1.0 %, the failure load $P_{f\,(EXP)}$ increased by 24%, 17%, and 23% for groups A, B, and C, respectively. The average increase in $P_{u(EXP)}$ is 21%. As l_f/ϕ_f ratio was increased from 0 to 80 with constant fibre content as 1%, $P_{u(EXP)}$ was higher by 23.5% for group A, by 14.2% for group B, and by 22.4% for group C. The mean increase in $P_{u(EXP)}$ is 20%. Also, the increase of fibre content V_f or fibre aspect ratio l_f/ϕ_f delays the appearance of the first diagonal shear cracks, especially for deep beams with a/d > 0.44. For non-fibrous deep beams, the ratio between cracking shear load and failure load P_{crs} / $P_{f\,EXP}$ was 0.48 in group B and 0.65 in group C. For constant l_f/ϕ_f as 80 in Group C, P_{crs} / $P_{u\,EXP}$ ratio is 0.55 for V_f = 0.5% and 0.75 for V_f = 1.0%. For constant V_f as 1% in Group B, P_{crs} / $P_{u\,EXP}$ ratio is 0.57 for l_f/ϕ_f = 60 and 0.58 for l_f/ϕ_f = 80. The measured deflections indicate that beams with higher fibre content V_f or fibre aspect ratio l_f/ϕ_f exhibit less deformation as the existing of steel fibres bridge and arrest the concrete cracks under applied stresses. As V_f increased from 0.0% to 1.0%, the final deflection was reduced by 34%, 21%, and 19% for groups A, B, and C, respectively.

The average decrease in Δ_f is 25%. The increase of fibre aspect ratio l_f/ϕ_f from 0 to 80 with 1% fibre content, results in reduction of the final deflection Δ_f by 34.4%, 42.4 % and 20.0 % for groups A, B, and C respectively. The mean decreases in Δ_f is 32%. Also, the increases of the fibre aspect ratio l_f/ϕ_f enhance the displacement ductility and energy absorption performance. As V_f increased from 0.0% to 1.0%, displacement ductility was increased by 23%, 37%, and 44% for groups A, B, and C, respectively. The average increase of the displacement ductility $\phi_{\Delta f}$ is 35%. The increase of the fibre aspect ratio from 0 to 80 increases the displacement ductility $\phi_{\Delta f}$ by 23.2%, 36.5% and 43.6 % for groups A,B and C respectively. The mean increase of the displacement ductility $\phi_{\Delta f}$ is 34%.

For different values of shear span-to-depth ratio a/d, the measured load-deflection curves are drawn in Fig. 8 for beams A1, A3, B1, B3, C1, and C2. Figure 8 shows that the decrease of shear span-to-depth ratio a/d leads to an increase in the load carrying capacity at different levels as a result of

enhanced arching action. As *a/d* ratio decreased from 1.00 to 0.44 the failure load increased by 70%. Also, the first diagonal shear crack load was increased by 25%. The measured deflections show that beams with smaller shear span-to-depth ratio *a/d* ratio exhibit less deformation. As *a/d* ratio decreased from 1.00 to 0.44, the deflection at failure load was decreased by an average value 61%. The displacement ductility varied depending on *a/d* ratio; the lower *a/d* ratio the lower amount of displacement ductility. As *a/d* ratio decreased from 1.00 to 0.44, the displacement ductility decreased by an average value 56%.

To study the effect of web reinforcement inclusion, Fig. 9 and Fig. 10 show the measured load-deflection curves for groups H and V, respectively. Generally, the load carrying capacity of the deep beams increases with the increase of horizontal or vertical stirrups ratio. The improvement in load carrying capacity is due to the effective role of web reinforcement in restricting the diagonal cracks width development. The increase of ρ_h from zero to 0.84% and 1.68%, increases the failure load $P_{f(EXP)}$ by 1.86% and 3.20% for beams H2 and H1, respectively. The increase of ρ_v from zero to 0.84% and 1.68%, enhances the failure load $P_{f(EXP)}$ by 1.92% and 3.02% for beams V2 and V1, respectively. Also, the increase of horizontal or vertical stirrups ratio leads to a decrease in deflection at failure and to an increase in displacement ductility $\phi_{\Delta f}$. The increase of ρ_h or ρ_v from zero to 0.84% and 1.68% decreases the maximum deflection by 16.7% and 24.8% respectively for beams H2 and H1, and by 11.5% and 14.53% respectively for beams V2 and V1. Same increase in web reinforcement increases the displacement ductility $\phi_{\Delta f}$ by 4.1% and 12.3% respectively for beams H2 and H1, and by 2.1% and 10.4% respectively for beams V2 and V1. The results of specimens H3 and V3 indicate that the horizontal web steel is more efficient in shear resistance than the vertical web reinforcement. At failure, the load carrying capacity for specimen H3 is higher than that for specimen V3 by 3.0%.

3.3 Steel strains

For all beams, the strain in the longitudinal main steel is given in Table 2 at yield level ε_y, at ultimate level ε_u, and at failure ε_f. Also, the strain ductility of critical beam section $\phi_{\varepsilon f}$ is given and calculated as the ratio between the strain at failure and the yield strain

$$\phi_{\varepsilon f} = \varepsilon_f / \varepsilon_y \quad (2)$$

Figure 11 shows the effect of fibre volume on the measured load- longitudinal steel strain curves for beams A0, A1, A3, C0, C1 and C2, respectively with fibre content 0.0, 0.5% and 1.0%. The effect of fibre aspect ratio l_f/ϕ_f on the measured load- longitudinal steel strain response is illustrated in Fig. 12 for beams A0, A2, A3, B0, B2 and B3. The fibre aspect ratio was 0.0, 60 and 80. It is clear that increasing the fibre volume or the fibre aspect ratio has a minor effect on the improvement of the ascending branch of the measured curves of tested beams. The slight increase in the slope for curves with the higher V_f or l_f/ϕ_f is due to the enhanced tension stiffening effect associated with the inclusion of steel fibres. The effect of increasing fibre content or fibre aspect ratio is mainly clear in the post-yield regime. As fibre volume V_f increased, and also the steel strain corresponding to the failure load increased, and strain ductility increased.

The effect of shear span-to-depth ratio *a/d* is studied in Fig. 13 for beams A0, A1, A3, B0, B1, B3, Co, C1 and C2. The decrease of shear span-to-depth ratio *a/d* leads to decrease the tensile strain in steel reinforcement at different load levels. As expected, the increase of *a/d* ratio increases the flexural effect on the beam response and consequently increases the steel strain and strain ductility. The slope of the load- longitudinal steel strain curves is significantly increased for beams with lower *a/d* ratio. This improvement is due to the enhanced arching action effect.

3.4 Concrete surface strains

Figure 14 shows typical measured load-concrete strain relationships. It is clear that the increase of the steel fibre volume V_f or fibre aspect ratio l_f/ϕ_f increases the maximum measured strain of concrete. As V_f increased from 0.5 to 1.0% the maximum strain of concrete increased by 29.0%. Also, as l_f/ϕ_f increase from 60 to 80, the maximum strain of concrete is increased by 14.3%.

Typical flexural strain distribution profiles for some deep beam specimens are drawn in Fig. 15. These profiles were drawn at 80% of failure load for critical of sections at mid-span. The strain distribution is nonlinear. The compression strain at the top fibre increases as the load increases, but in the tension zone the various recorded values were disturbed by the cracks and the flexibility of this area. The concrete strain measurements in the tension zone are not accountable and the steel strain is

only governed. The neutral axis has a changeable depth till the failure. The upward movement of neutral axis is associated with the cracking progress under load increasing.

4 Finite Element Modeling and Results

4.1 Finite element discretization for deep beams

The tested deep beams have been analyzed using finite element FE program; ANSYS 15 [37]. In nonlinear analysis, the total load applied to the FE model is divided into a series of load increments. For each load increment, the iterative solution performed was the standard Newton-Raphson technique. The load increment was set at 5% of the experimental failure load. The load increment was subject to adjustment to obtain results at certain specific load levels. The maximum number of iterations was set to 50 in each load step and the equilibrium tolerance of 0.5% was chosen. In the finite element discretization of each beam, a mesh of 25 x 25 x 25 mm size of eight-node elements (Solid 65) was used for concrete. The top and bottom flexural steel bars, the horizontal and the vertical web reinforcement were represented by discrete bar element (Link 8). A (Solid45) element was used for steel plates at the supports and loading of the tested beam.

4.2 Constitutive modeling of steel fibre concrete

Figure 16 shows the simplified uniaxial stress strain curve; used here for fibre concrete in compression. It was clear from the figure the role of the steel fibre in increasing the compressive strength of concrete. The stress-strain curve is linearly elastic up to about 30 percent of the maximum compressive strength. In this stage, the elasticity modulus is measured by the initial tangent modulus E_{ci}. The value of the initial tangent modulus of elasticity, (E_{ci}) is given by Egyptian code [2] as:

$$E_{ci} = 4400\sqrt{f_{cu}} \quad (3)$$

Where f_{cu} is the compressive strength of concrete in MPa

Above the elasticity stage, the stresses increase gradually up to the maximum compressive strength f_{cuf} and corresponding strain εcf using parabolic function [42]. Then, the curve descends into a softening region, and eventually crushing failure occurs at an ultimate strain ε_{cuf}. In the present work, the constitutive compression law in ANSYS program was modified to include the effects of steel fibres inclusion on the mechanical properties of concrete. The strain at peak compressive stress - crushing strain- ε_{cuf} tends to increase due to the presence of steel fibre [39]:

$$\varepsilon_{cuf} = 0.0021 + 0.007\frac{V_f\, l_f}{\phi_f} \quad (4)$$

Also, the following linear regression equation was derived to predict compressive strength of HSSFRC (High Strength Steel Reinforced Concrete) composite f_{cuf} as:

$$f_{cuf} = f_{cu}\left(1 + 0.1066\frac{V_f\, l_f}{\phi_f}\right) \quad (5)$$

The behavior of fibrous concrete in tension is represented by the stress-strain relation as shown in Fig. 17. Before cracking, the stress-strain relation is assumed to be linear till the tensile strength of concrete. The slope of this linear part is defined as modulus of elasticity of fibrous concrete E_{cf} in tension. The initial linear part is defined by the peak tensile strength f_{tf} . The strain corresponding to peak stress ε_{tp} which is defines the crack initiation, is given by

$$\varepsilon_{tp} = f_{tf} / E_{cf} \quad (6)$$

The peak tensile strength of HSSFRC composite (f_{tf}) (in MPa) [39]:

$$f_{tf} = f_t\,(1 + 0.016\, N_f^{1/3} + 0.05\pi\, \phi_f\, l_f\, N_f) \quad (7)$$

Where (f_t): tensile strength of concrete in MPa, and (N_f): number of fibres per unit cross section area and can be calculated from [39]:

$$N_f = \eta_o\,(4\, V_f / \pi\, \phi_f^{\,2}) \quad (8)$$

After cracking, a smeared model is used to represent the discontinuous macro-crack behavior. This cracked concrete can still carry some tensile stress perpendicular to the crack, which is termed tension stiffening. The tension stiffening factor (α_m) account for the pull-out resistance of fibrous concrete was taken as 0.6 [39]. A simple descending line is used to model this tension stiffening phenomenon as shown in Fig. 17. The default value of the strain ε_{tu} at which the tension stiffening stress reduced to zero is taken as 6 times the cracking strain. For the concrete, when the tensile stress in the principle direction exceeds the tensile strength of concrete, f_{tf}, the tensile failure would occur [40]. After the crack forms, both normal and shear stiffness are reduced, the concrete cracks and the strength decreases gradually to zero. A shear transfer coefficient β_t, is introduced which represents a shear strength reduction factor for cracked concrete. Shear transfer coefficients are taken 0.30 for open crack and 0.75 for closed crack.

The failure surface developed for plain concrete [41] has been modified to account for the presence of steel fibres. Fig. 18 shows a schematic failure surface of concrete in three-dimensional stress spaces. The figure shows that the steel fibres offer higher confinement which increases the strength of concrete. The failure envelope is smooth, convex and its deviatoric sections become more circular in shape for increasing hydrostatic pressures. Consequently, a criterion for failure of the concrete due to a

multiaxial stress state can be calculated. In a concrete element, cracking occurs when the principal tensile stress in any direction lies outside the failure surface. The limiting tensile stress required to define the onset of cracking can be calculated for states of triaxial tensile stress and for combinations of tension and compression principal stresses. The stress function adopted in the present work has been used by William and Warnke [42].

4.3 Finite element results

The ANSYS program records cracks at each applied load step. Fig[s]. 19 to 21show evolutions of crack patterns developing for each beam at the last loading step. ANSYS program displays circles at locations of cracking or crushing in concrete elements. Cracking is shown with a circle outline in the plane of the crack, and crushing is shown with an octahedron outline. The first crack at integration point is shown with a red circle outline (actually vertical red line indicates the flexural crack and the inclined red line indicates diagonal shear crack), the second crack with a green outline (inclined secondary crack), and the third crack with a blue outline (excessive flexural crack) [41]. The computed cracking patterns at different loading levels are presented for the tested beams A2, B2, and C2, respectively in Fig[s]. 19, 20 and 21. The predicted crack patterns and the failure modes are in a good agreement with the experimental results. Generally, the simulation predicts first flexural cracking at mid-span. With further load increase, the diagonal shear cracks were developed and increased gradually. The first shear crack was appeared at load level as 530, 507 and 445 kN for beams A2, B2, and C2 respectively. After the formation of the crack band, a rather stable crack pattern is formed. Also, the shear crack band seems to increase in width with an increase of the load. Ultimately, failure is initiated by crushing of the concrete in the region adjacent to the upper of mid-span. For beam A2, the predicted failure load is 1325 kN and the mode of failure is shear-compression failure. For beam B2, the predicted failure load d is 702 kN and the mode of failure is diagonal-splitting failure. Finally, for beam C2, the predicted mode of failure is crushing of concrete strut at failure load equal 555 kN.

In Table 3, the numerical results for the loads and the corresponding deflections are given at the first shear cracking and failure levels. Figure 22 shows the load-deflection plots from the finite element analysis and the experimental results for beams A2, A3, B2, and C2. The load-deflection response is generally predicted well. Furthermore, the analysis reflects the significance of the investigated test parameters. The average failure load from the experimental results was 1.10 of the numerical models. The average value of the ratio between the first shear cracking load and the failure load $P_{crs} / P_{u(EXP)}$ was 0.50 for the testing results, and 0.55 for numerical results. For deflections at failure, the average

ratio of $\Delta_{f(FE)}/\Delta_{f(Exp)}$ is 1.12%. The measured deflections indicate that beams with smaller (a/d) ratio or the beams with bigger values of V_f or l_f/ϕ_f, exhibit less deformation.

The predicted load-strain curves for the bottom longitudinal steel are compared with the measured results for beams A1, A2, C2 and V2 as shown in Fig. 23. There is a reasonable agreement between the experimental and the numerical load-strain curves. Generally, at early loading level, the load-steel strain relation is linear up to primary shear cracking (cracking point). Then, the curve increases gradually with less slope until yielding of the reinforcing steel bars is reached (yielding point). Between the yield point and the failure point, there is a little increase in the load carrying capacity with a significant increase in steel strain as shown in Fig. 24. The cracking and yielding points occur respectively at 24% and 88% of failure load. As can be seen, excellent agreement is obtained between experiment and simulation. Based on comparison of the computed numerical results with the available experimental ones, it is verified that the finite element method and materials models used in utilizing ANSYS computer program are reliable and accurate to predict the behavior of nonlinear geometric and nonlinear material behavior of steel fibres reinforced concrete deep beams.

5 CONCLUSIONS:

From the experimental and numerical results for steel fibre high strength reinforced concrete deep beams in the present work, the following conclusions are drawn:

1. Generally, the failure modes of all tested specimens are shear accompanied with clear vertical and diagonal cracks. The failure modes for deep beams without fibres were brittle failure modes; namely shear-compression and crushing of strut. As fibre volume content V_f and fibre aspect ratio l_f/ϕ_f is increased, the mode of failure changes from sudden brittle failure mode to less brittle failure mode which is called diagonal-splitting failure mode. Also, the results show that the strain distribution profiles are nonlinear for all tested specimens.

2. The increase in fibre volume content V_f or fibre aspect ratio l_f/ϕ_f leads to an increase in the failure load $P_{f(EXP)}$, the first diagonal cracking load P_{crs}, the displacement ductility $\phi_{\Delta f}$ and the steel strain corresponding to the failure load while it reduces the deflection at failure load Δ_f. For fibre content V_f = 1%, the average increase in $P_{u(EXP)}$, P_{crs}, and $\phi_{\Delta f}$ was 21%, 32% and 35% , respectively compared to the control specimen without fibre and the mean reduction in Δ_u was 25%. The change of fibre aspect ratio l_f/ϕ_f from zero to 80 increases P_{crs} by 32%, $P_{u(EXP)}$ by 4% and $\phi_{\Delta f}$ by 34%, while it decreases Δ_u by 12%.

3. The decrease of shear span-to-depth ratio *(a/d*) enhances the failure load and first diagonal shear crack P_{crs}, while it reduces the displacement ductility $\phi_{\Delta f}$ and the deflection at failure load Δ_f This improvement is due to the enhanced arching action effect. The change of *(a/d*) ratio from 1.00 to 0.44 increases $P_{u(EXP)}$ by 70%, P_{crs} by 25%, while decreases $\phi_{\Delta f}$ by 56 % and Δ_f by 61 %. The decrease of (*a/d)* ratio leads to decreasing the tensile strain in steel at different load levels.

4. The increase of horizontal stirrups (ρ_h) or vertical stirrups *(*ρ_v) improves the failure load $P_{f\,(EXP)}$, and the displacement ductility $\phi_{\Delta f}$, while it reduces the deflection at failure load Δ_f. The increase of ρ_h from zero to 1.68% increases $P_{u(EXP)}$ by 3.20%, improves $\phi_{\Delta f}$ by 12.33%, and decreases Δ_u by 24.84%. The increase of ρ_v from zero to 1.68%, enhances $P_{u(EXP)}$ by 3.0%, rises $\phi_{\Delta f}$ by 10.35%, and decreases Δ_u by 14.53%. It is clear that the horizontal web steel reinforcement is slightly more efficient in shear resistance than the vertical web reinforcement.

5. The predicted numerical results from ANSYS program for loading and deflection at failure and at first cracking levels, show good agreement with the experimental results. Also, the simulated cracking patterns and failure modes are nearly similar to the testing results for all beams. The average ratio between the measured load and predicted load is 0.91 at first diagonal crack level, and 1.1 at failure level. Finally, the average ratio between numerical and experimental deflection at failure load values is 1.12.

6 NOTATIONS

a = shear span (the distance from the load to the support);
a/d = shear span to depth ratio;
b = beam width = 120 mm;
d = the beam effective depth = total depth- concrete cover;

E_{ci} = elasticity modulus of fibrous concrete in compression;
E_{cf} = elasticity modulus of fibrous concrete in tension = $f_{tf} / \varepsilon_{tf}$;
E_s = Elastic modulus of the steel reinforcement;
E_c = Elastic modulus of the normal concrete;
f_{cu} = compressive strength of normal concrete;
f_{cuf} = compressive strength of high strength fibre reinforced concrete
f_t = tensile strength of normal concrete;
f_{tf} = tensile strength of high strength fibre reinforced concrete;
f_f = reinforcing steel stress at failure;
h = height (total depth) of the beam;
L = outer beam span length;
L_e = inner beam span length from center lines of supports;
L_n = length of clear span measured face-to-face of supports;
l_f = the length of the steel fibre;
l_f/ϕ_f = the aspect ratio of the steel fibres;
n = modular ratio = E_s/E_c = 10;
P_{crs} = first diagonal cracking load;
$P_{f(Exp)}$ = failure experimental strength;
S_v = spacing of vertical web reinforcement = 50,75,100 mm;
S_h = spacing of horizontal web reinforcement = 50,75,100 mm;
V_f = volume of the steel fibre/volume of the R.C
W/C = water/cement ratio ;
α_m = tension stiffening factor = 0.6 [39];
β_t = shear strength reduction factor for cracked concrete;
$\Delta_{f(Exp)}$ = experimental deflection at the experimental failure load;
$\Delta_{f(FE)}$ = numerical deflection at the numerical failure load;
Δ_y = deflection at the yield level;
ε_{cf} = corresponding strain at maximum compressive strength of fibrous concrete;
ε_{cuf} = corresponding strain at crushing failure of fibrous concrete;
ε_f = steel strain at failure;
ε_{tp} = corresponding strain at peak tensile stress of fibrous concrete;
ε_{tf} = corresponding strain at tensile strength of high strength fibrous concrete;
ε_{tu} = corresponding strain at zero tension stiffening stress for fibrous concrete;
ε_t = corresponding strain at zero tension stiffening stress for normal concrete;
ε_u = steel strain at ultimate stress;
ε_{su} = corresponding strain at ultimate stress of the reinforcing steel;
ε_y = steel strain at yield load;
$\phi_{\Delta f}$ = displacement ductility of each beam;

ϕ_{ef} = strain ductility of the beam at critical section;

ϕ_f = diameter of the steel fibres;

σ_1 , σ_2 , σ_3 = hydrostatic axes;

η_o = fibre orientation factor;

ρ_h = percentage of horizontal shear reinforcement = $(n_h \cdot A_{sh})/(b*s_h) * 100$;

ρ_s = main tension steel ratio;

ρ_v = percentage of vertical shear reinforcement= $(n_v \cdot A_{sv})/(b*s_v) * 100$;

n_v = number of branched of the vertical stirrups = 2;

n_h = number of branched of the horizontal stirrups = 2;

A_{sv} = area of one branch of the vertical stirrups = $\pi \Phi^2_v/4 = 50.27$ mm^2;

A_{sh} = area of one branch of the horizontal stirrups = $\pi \Phi^2_h/4 = 50.27$ mm^2; ;

Φ_v = the diameter of the vertical stirrups = 8 mm;

Φ_h = the diameter of the horizontal stirrups = 8 mm;

Table 1 Details of tested deep beams.

Group No.	Beam	a (mm)	L_e (mm)	a/d	V_f (%)	l_f/ϕ_f	S_v (mm)	ρ_v (%)	S_h (mm)	ρ_h (%)
1	A0	200	700	0.44	0.00	0	75	1.12	75	1.12
	A1	200	700	0.44	0.50	80	75	1.12	75	1.12
	A2	200	700	0.44	1.00	60	75	1.12	75	1.12
	A3	200	700	0.44	1.00	80	75	1.12	75	1.12
2	B0	365	900	0.81	0.00	0	75	1.12	75	1.12
	B1	365	900	0.81	0.50	80	75	1.12	75	1.12
	B2	365	900	0.81	1.00	60	75	1.12	75	1.12
	B3	365	900	0.81	1.00	80	75	1.12	75	1.12
3	C0	450	1000	1.00	0.00	0	75	1.12	75	1.12
	C1	450	100 0	1.00	0.50	80	75	1.12	75	1.12
	C2	450	1000	1.00	1.00	80	75	1.12	75	1.12
4	H1	365	900	0.81	1.00	80	75	1.12	50	1.68
	H2	365	900	0.81	1.00	80	75	1.12	100	0.84
	H3	365	900	0.81	1.00	80	75	1.12	0	0.00
5	V1	365	900	0.81	1.00	80	50	1.68	75	1.12
	V2	365	900	0.81	1.00	80	100	0.84	75	1.12
	V3	365	900	0.81	1.00	80	0	0.00	75	1.12

Table 2 The expiremntal results of all specimens.

Groups No.	Specim	P_{crs} (kN)	$P_{f(EXP)}$ (kN)	Δ_y (mm)	Δ_f (mm)	$\phi_{\Delta f} = \Delta_f / \Delta_y$	Failure mode	Yield strain	Ult. strain	Failure strain	Strain ductility
1	A0	350	1150	1.80	2.56	1.42	S.C.(1)	1.90	2.00	2.10	1.11
	A1	400	1350	1.46	2.22	1.52	C.S.(2)	2.08	2.08	2.50	1.20
	A2	400	1380	1.21	2.11	1.74	S.C.(1)	2.12	2.11	2.86	1.35
	A3	400	1420	0.96	1.68	1.75	S.C.(1)	2.20	2.14	3.08	1.40
2	B0	320	670	1.98	3.08	1.56	C.S.(2)	2.05	2.51	2.60	1.27
	B1	400	703.0	1.50	2.58	1.72	D.S.(3)	2.10	2.59	2.75	1.31
	B2	450	740.5	1.37	2.52	1.84	D.S.(3)	1.93	2.61	2.80	1.45
	B3	450	781.0	1.14	2.43	2.13	D.S.(3)	2.15	2.64	3.24	1.51
3	C0	320	490.0	2.25	3.66	1.63	D.S.(3)	2.31	2.71	3.11	1.35
	C1	300	550.0	1.69	3.35	1.98	D.S.(3)	2.28	2.77	3.24	1.42
	C2	450	600.0	1.25	2.93	2.34	C.S.(2)	2.31	2.82	3.55	1.54
4	H1	450	775	1.40	2.30	1.64	S.C.(1)	1.80	2.05	2.54	1.41
	H2	400	765	1.68	2.55	1.52	C.S.(2)	2.07	2.52	3.50	1.69
	H3	300	751	2.10	3.06	1.46	D.S.(3)	2.61	2.76	3.00	1.15
5	V1	450	750	1.58	2.53	1.60	C.S.(2)	2.22	2.74	3.10	1.40
	V2	400	742	1.77	2.62	1.48	D.S.(3)	2.30	2.76	3.40	1.48
	V3	350	728	2.04	3.15	1.54	C.S.(2)	2.10	2.57	2.77	1.32

Where:

S.C. (1) (Shear compression failure) ;

C.S. (2) (Crushing of concrete strut failure) ;

D.S. (3) (Daigonal splitting failure).

Table 3 Numerical results at different load levels.

Group No.	Specimen	$P_{crs(FE)}$ kN	$P_{F(FE)}$ kN	$\frac{P_{F(EXP)}}{P_{u(FE)}}$	$\frac{}{P_{crs(EX)}}$	$\frac{P_{crs(FE)}}{P_{F(FE)}}$	$\Delta_{u(FE)}$ (mm)	$\Delta_{u(EXP)}$ (mm)	$\frac{\Delta_{u(FE)}}{\Delta_{u(EXP)}}$
1	A0	412	1200	0.96	0.30	0.34	2.89	2.56	1.13
	A1	433	1320	1.02	0.30	0.33	2.55	2.22	1.15
	A2	424	1325	1.04	0.29	0.32	2.28	2.11	1.08
	A3	440	1350	1.05	0.28	0.33	1.86	1.68	1.11
2	B0	350	643	1.04	0.48	0.54	3.45	3.08	1.12
	B1	430	684	1.03	0.57	0.63	3.07	2.58	1.19
	B2	507	702	1.05	0.61	0.72	2.80	2.52	1.11
	B3	480	729	1.07	0.58	0.66	2.82	2.43	1.16
3	C0	330	468	1.05	0.65	0.71	3.99	3.66	1.09
	C1	335	495	1.11	0.55	0.68	3.72	3.35	1.11
	C2	445	555	1.08	0.75	0.80	3.34	2.93	1.14
4	H1	362	744	1.04	0.58	0.49	2.45	2.30	1.06
	H2	412	735	1.04	0.52	0.56	2.83	2.55	1.11
	H3	315	700	1.07	0.40	0.45	3.52	3.06	1.15
5	V1	370	705	1.06	0.60	0.52	2.82	2.53	1.12
	V2	410	693	1.07	0.54	0.59	2.93	2.62	1.12
	V3	455	684	1.06	0.48	0.67	3.57	3.15	1.13
Average				**1.10**	**0.50**	**0.55**			**1.12**

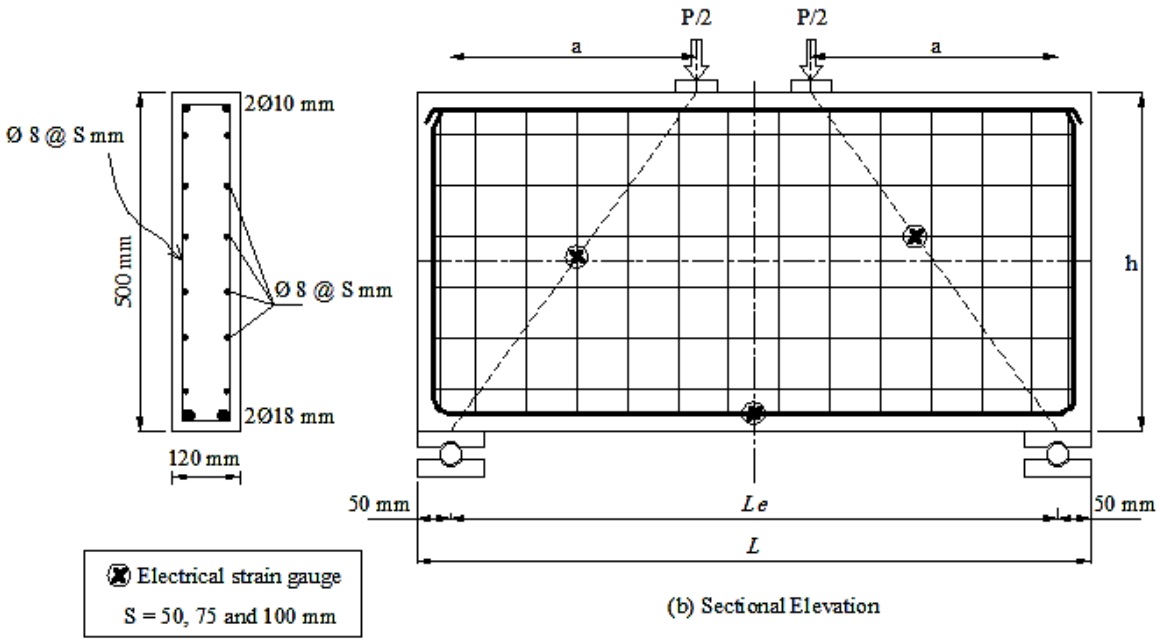

Fig. 1. Dimensions of the tested fibrous R.C deep beams.

Fig. 2. Photo of the test setup and instrumentations (Side View) .

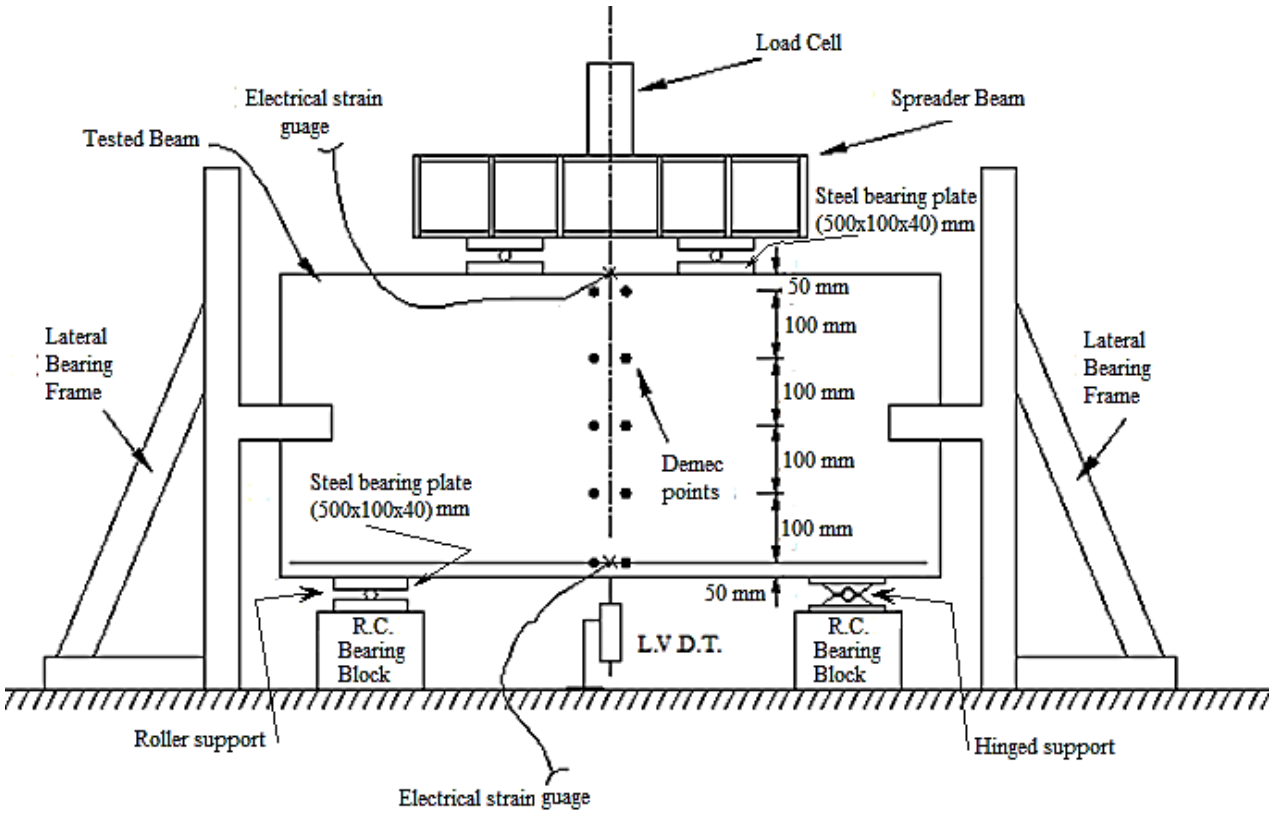

Fig. 3. Test setup and instrumentations.

(a) Specimen B1

(b) Specimen A1

(c) Specimen B2

(d) Specimen V2

(e) Specimen H2

Fig.4. Photos show the role of steel fibres to bridge and arrest the cracks.

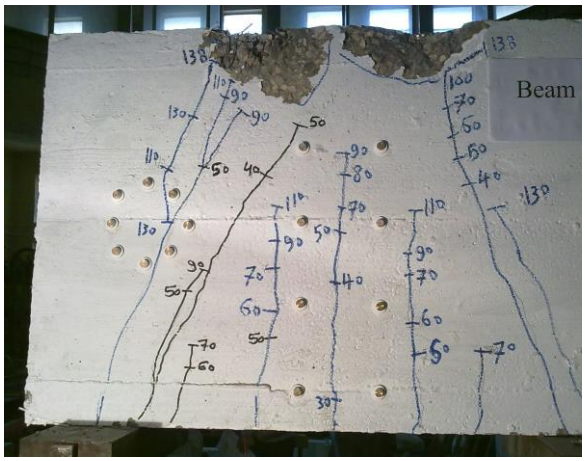

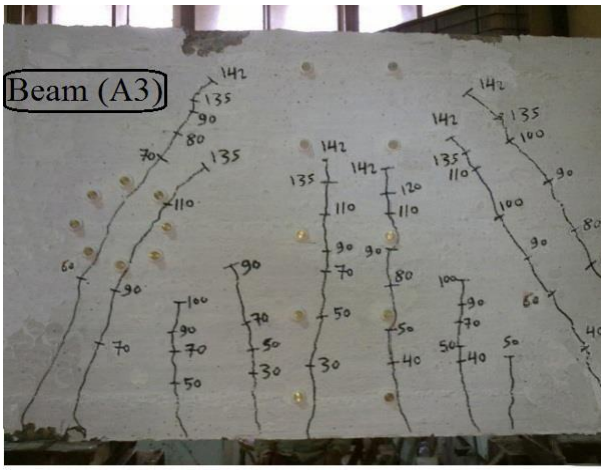

(a) Shear compression failure (S.C) specimen (A2) and (A3)

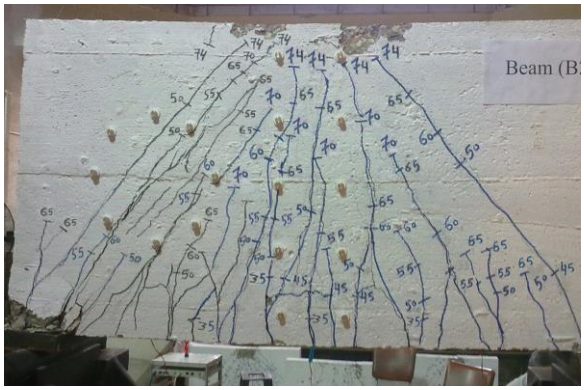

(b) Daigonal splitting failure (D.S) specimen (B2) and (C1)

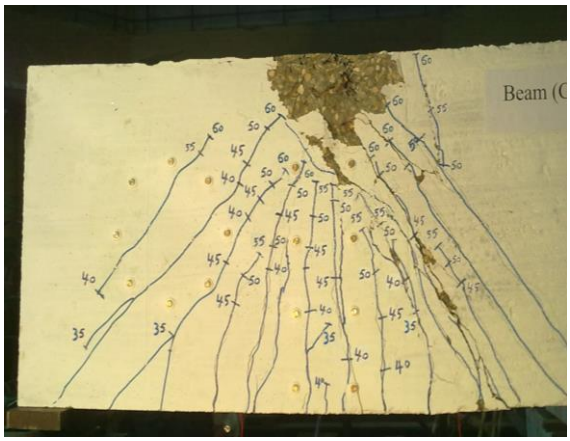

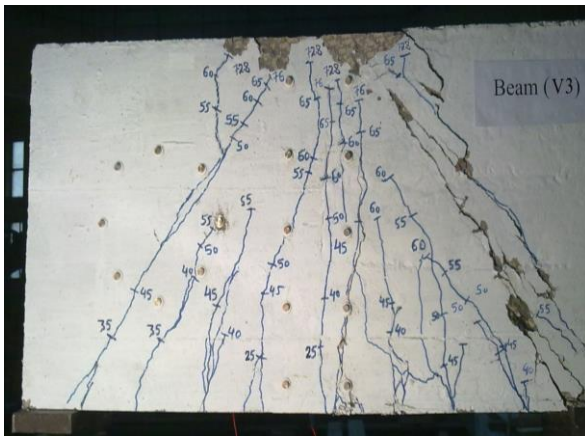

(c) Crushing of strut failure (C.S) specimen (C2) and (V3)

Fig. 5. Photos show the different modes of failure.

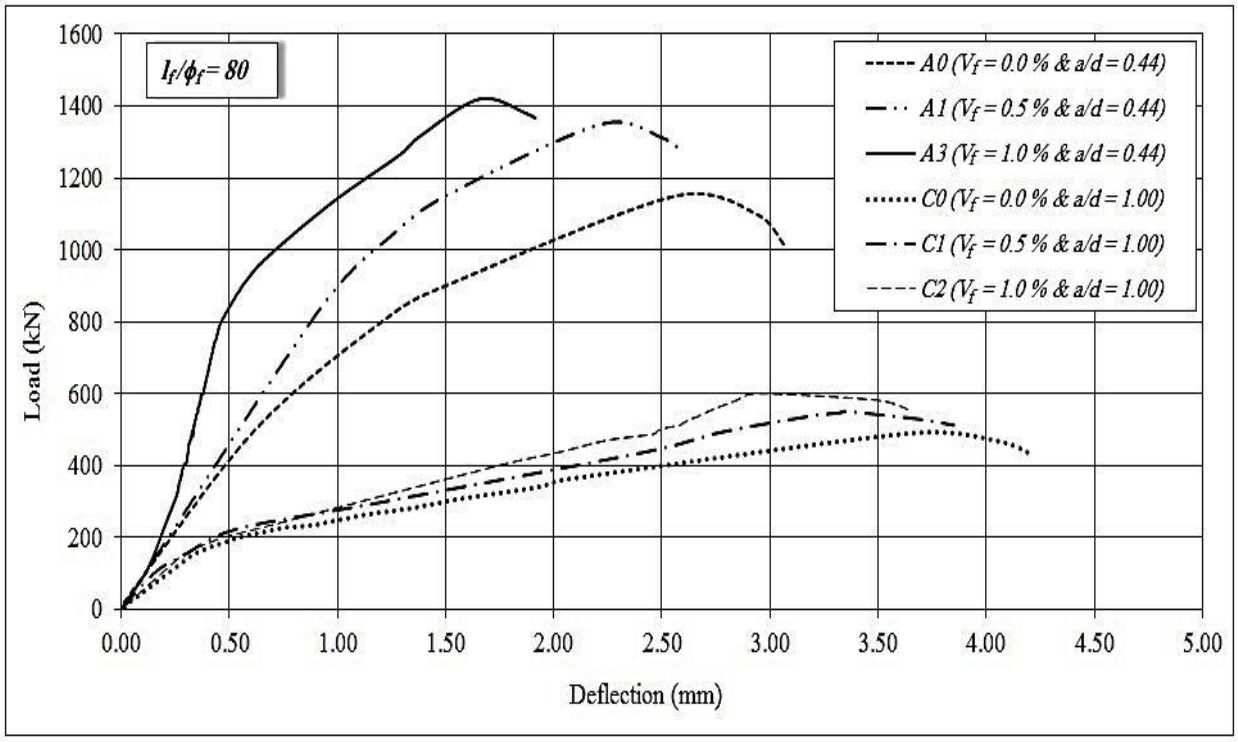

Fig. 6. Effect of the steel fibre volume content (Vf) on the load-deflection response.

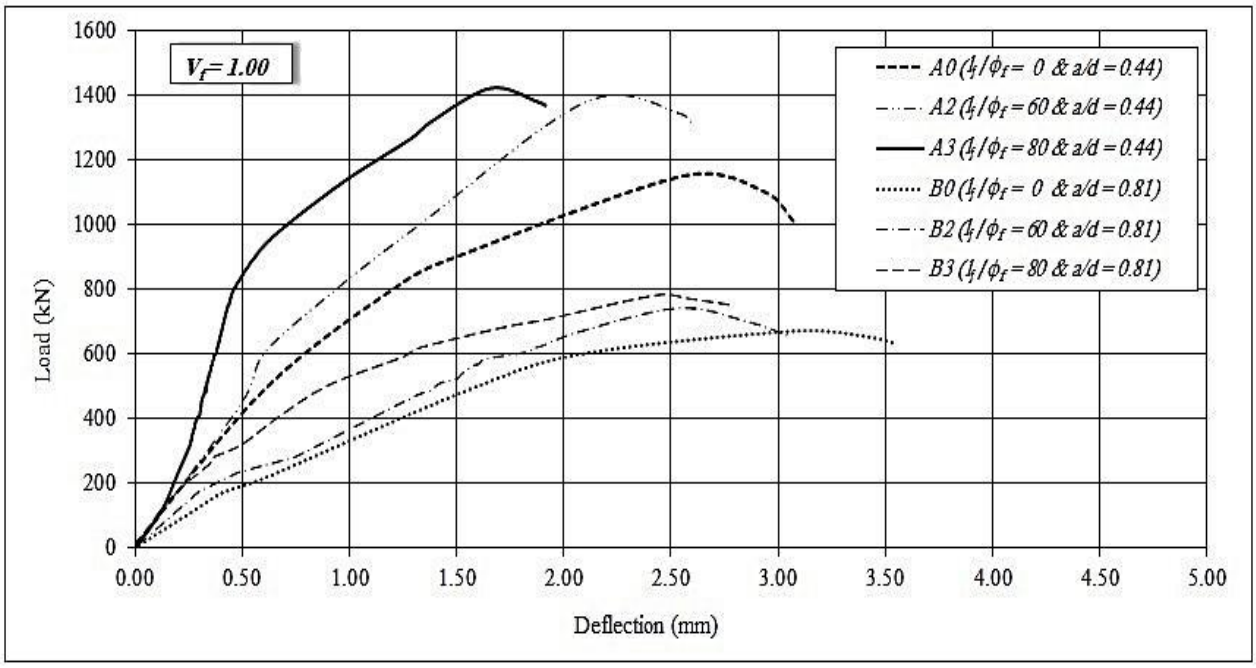

Fig. 7. Effect of the steel fibre aspect ratio (lf□□f) on the load-deflection response.

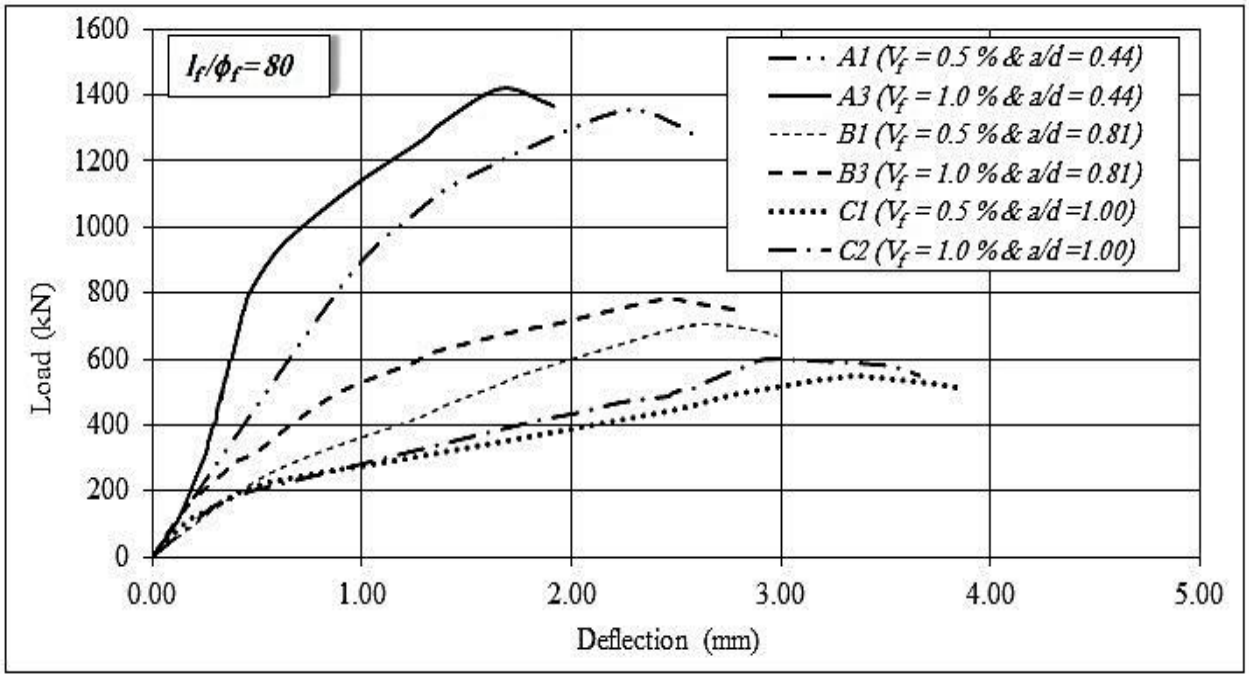

Fig. 8. Effect of shear span -to-depth ratio (a/d) on the load-deflection response.

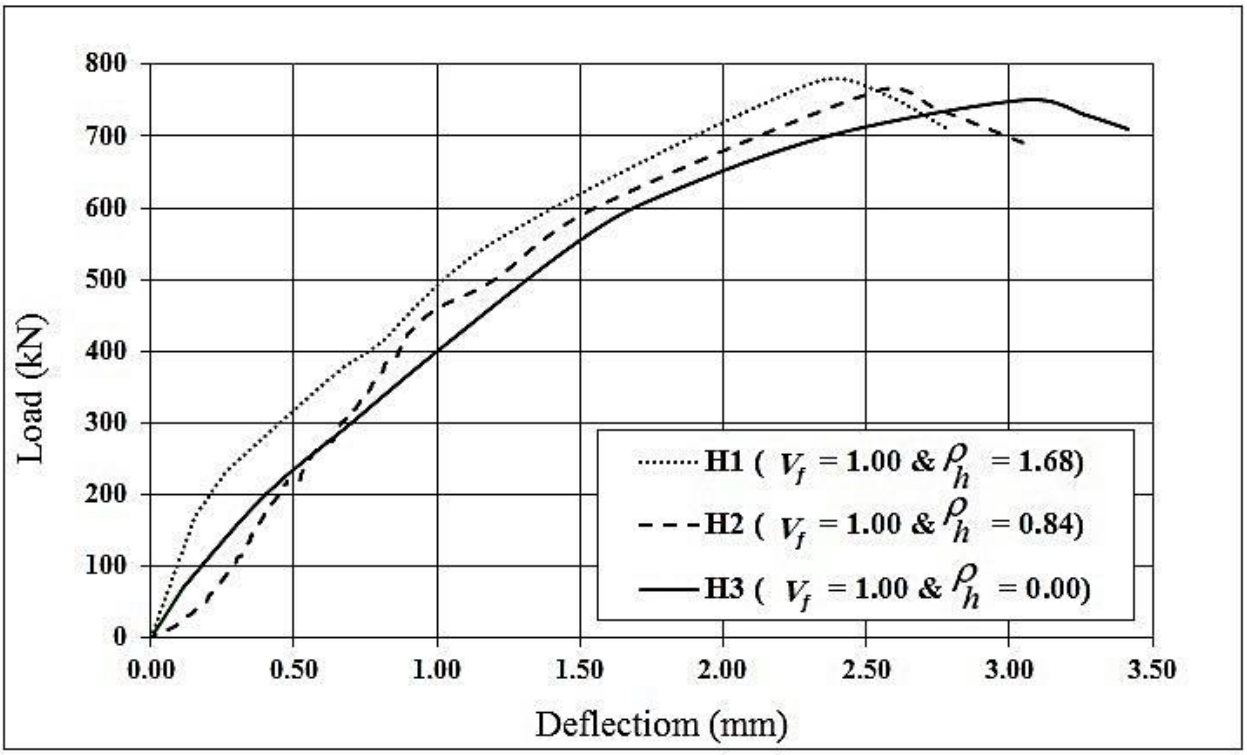

Fig. 9. Effect of horizontal web reinforcement on the load-deflection response group (H).

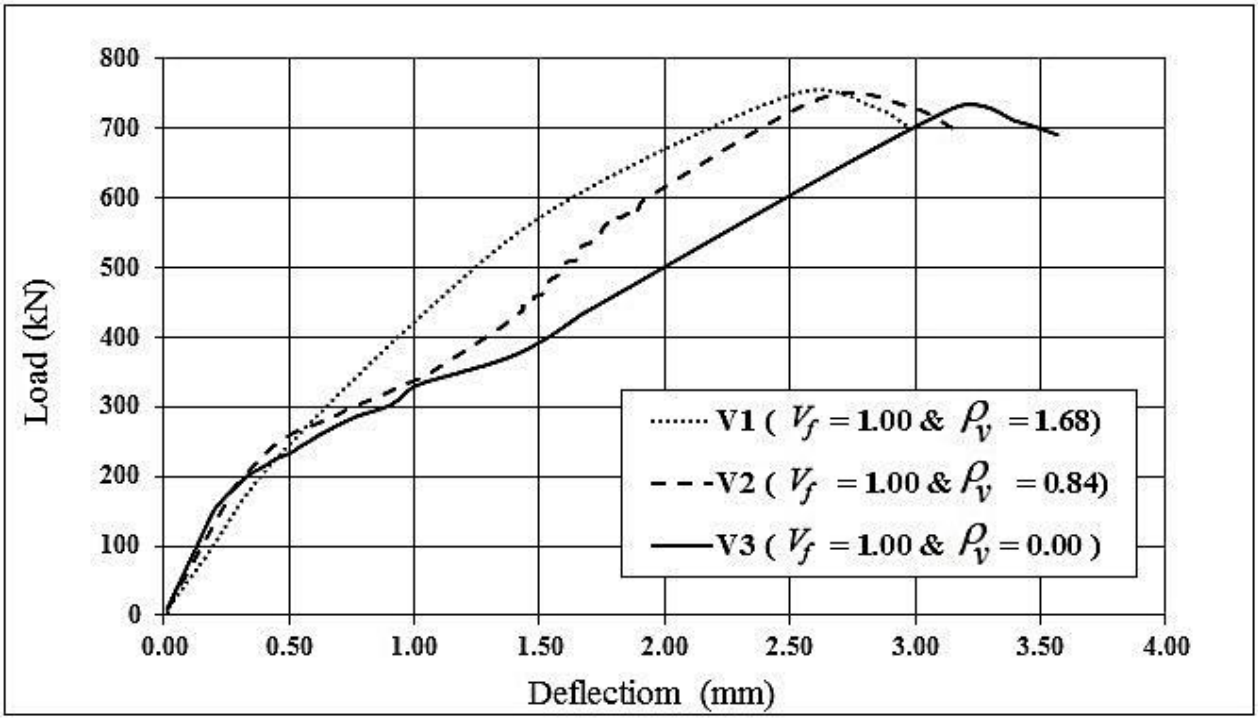

Fig. 10. Effect of vertical web reinforcement on the load-deflection response group (V).

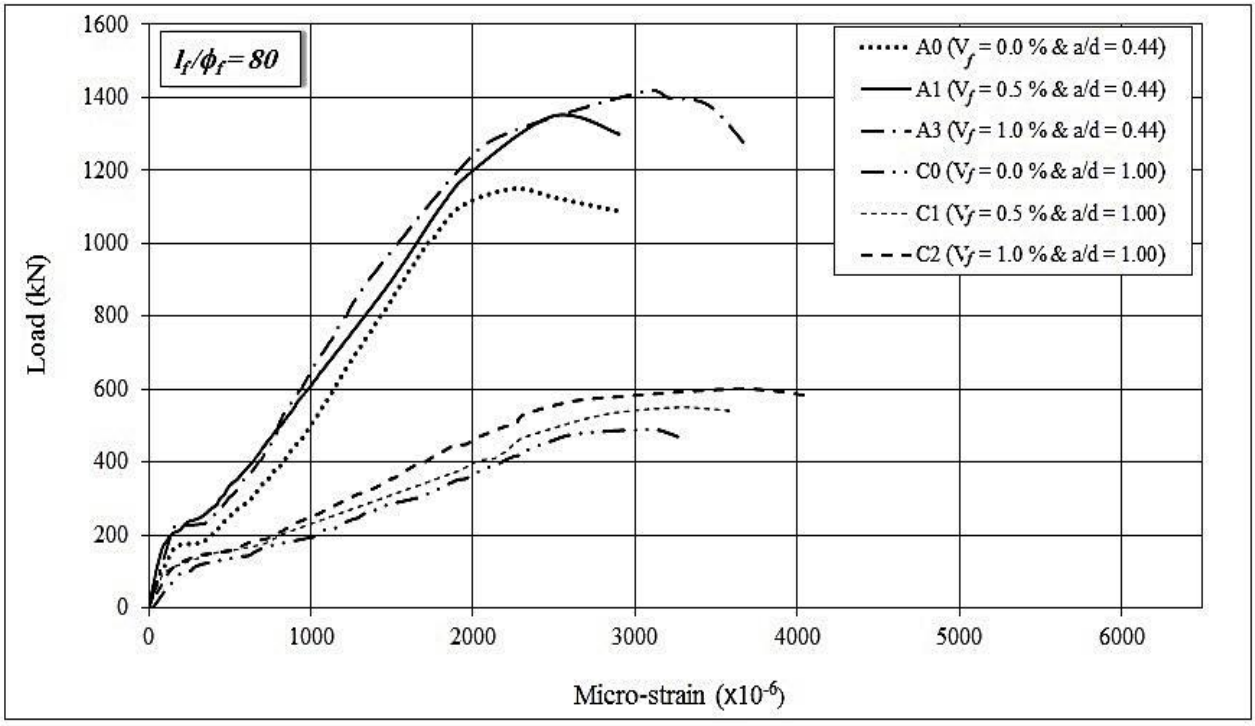

Fig. 11. Effect of the steel fibre volume content (Vf) on the load- steel strain response.

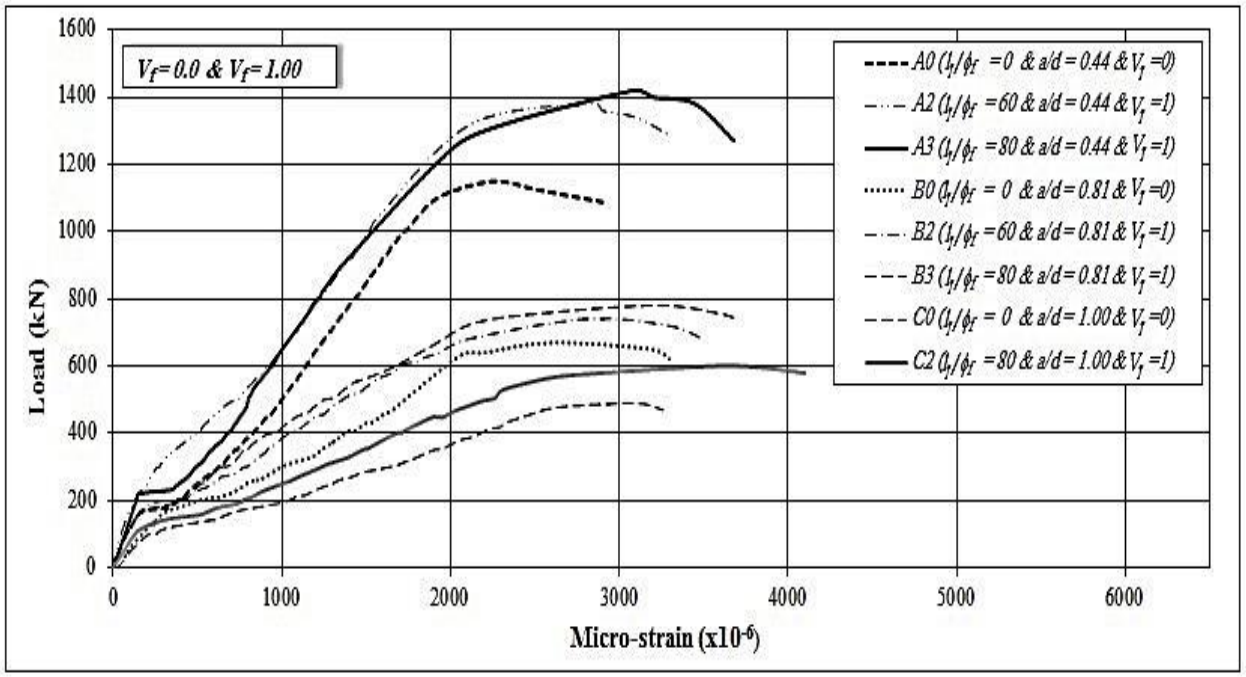

Fig. 12.a Effect of the steel fibre aspect ratio (lf□□f) on the load- steel strain response for Vf = 0.0 and Vf = 1.0 .

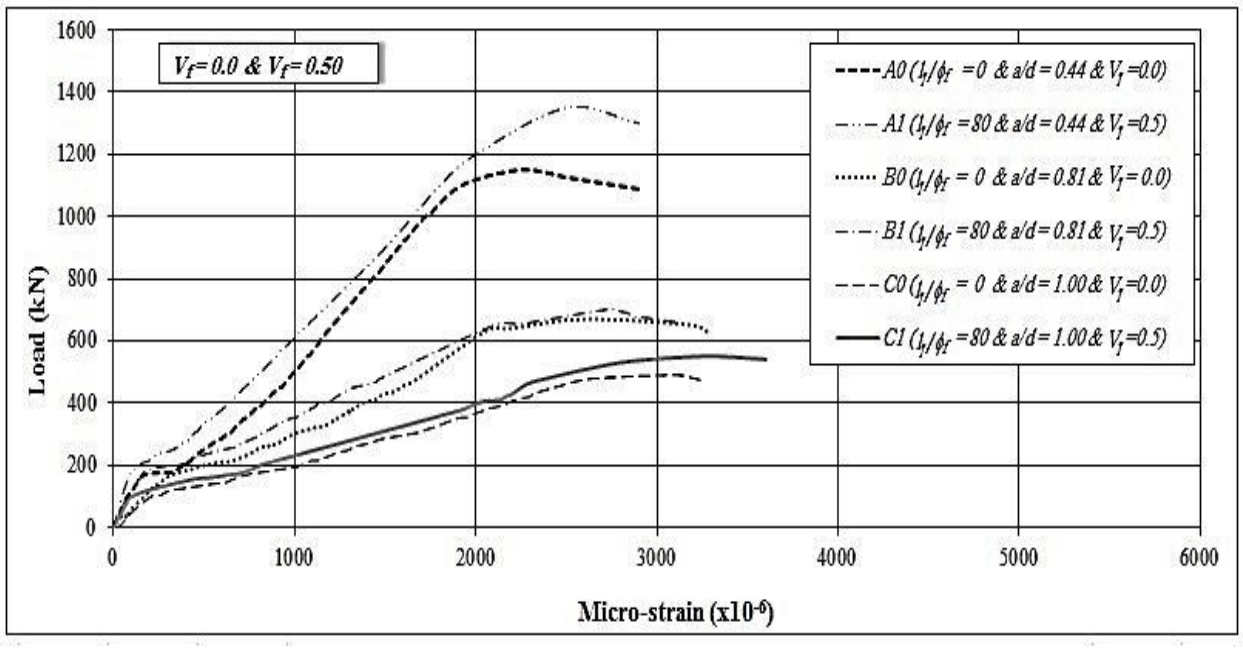

Fig. 12.b Effect of the steel fibre aspect ratio (lf□□f) on the load- steel strain response for Vf = 0.0 and Vf = 0.5.

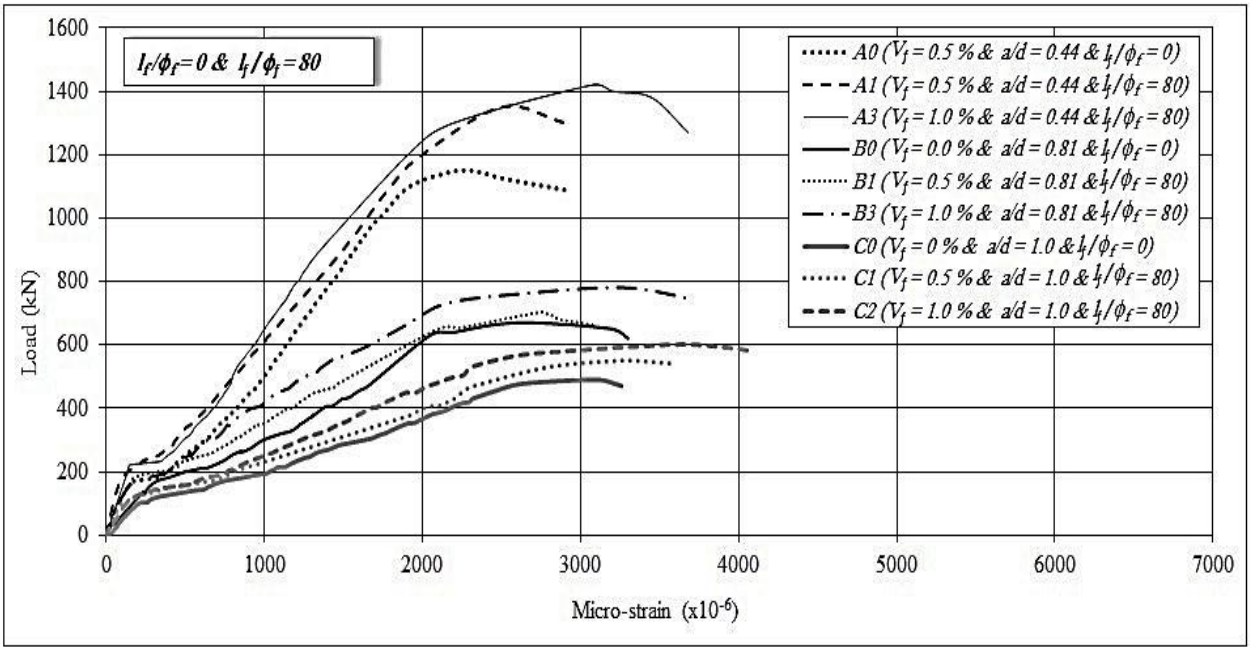

Fig. 13.a Effect of the steel fibre aspect ratio (lf□□f) on the load- steel strain response for (lf□□f) = 0.0 and (lf□□f) = 80 .

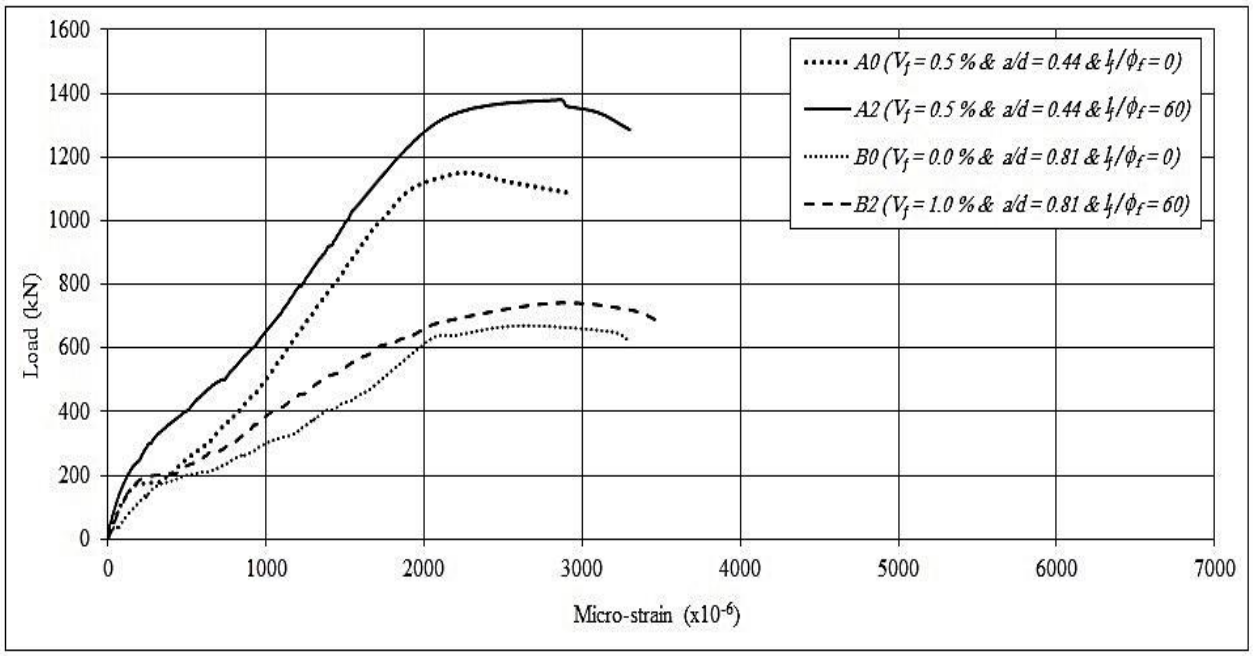

Fig. 13.b Effect of the steel fibre aspect ratio (lf□□f) on the load- steel strain response for (lf□□f) = 0.0 and (lf□□f) = 60 .

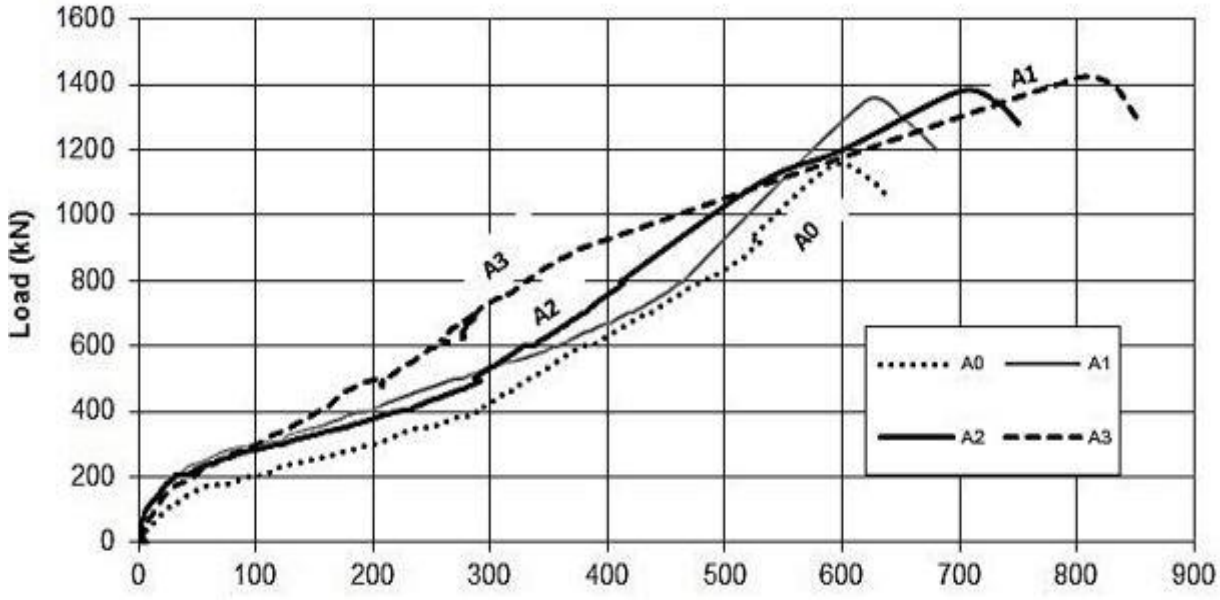

Fig. 14. Load - concrete strains in (10-5) for group (A) specimens.

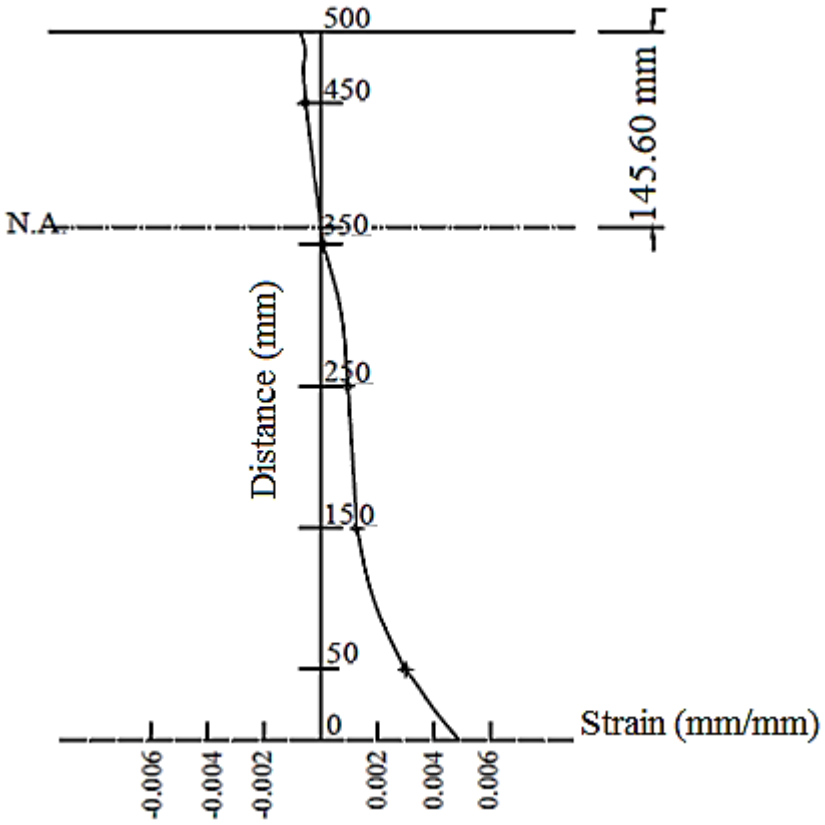

(a) Beam (A1).

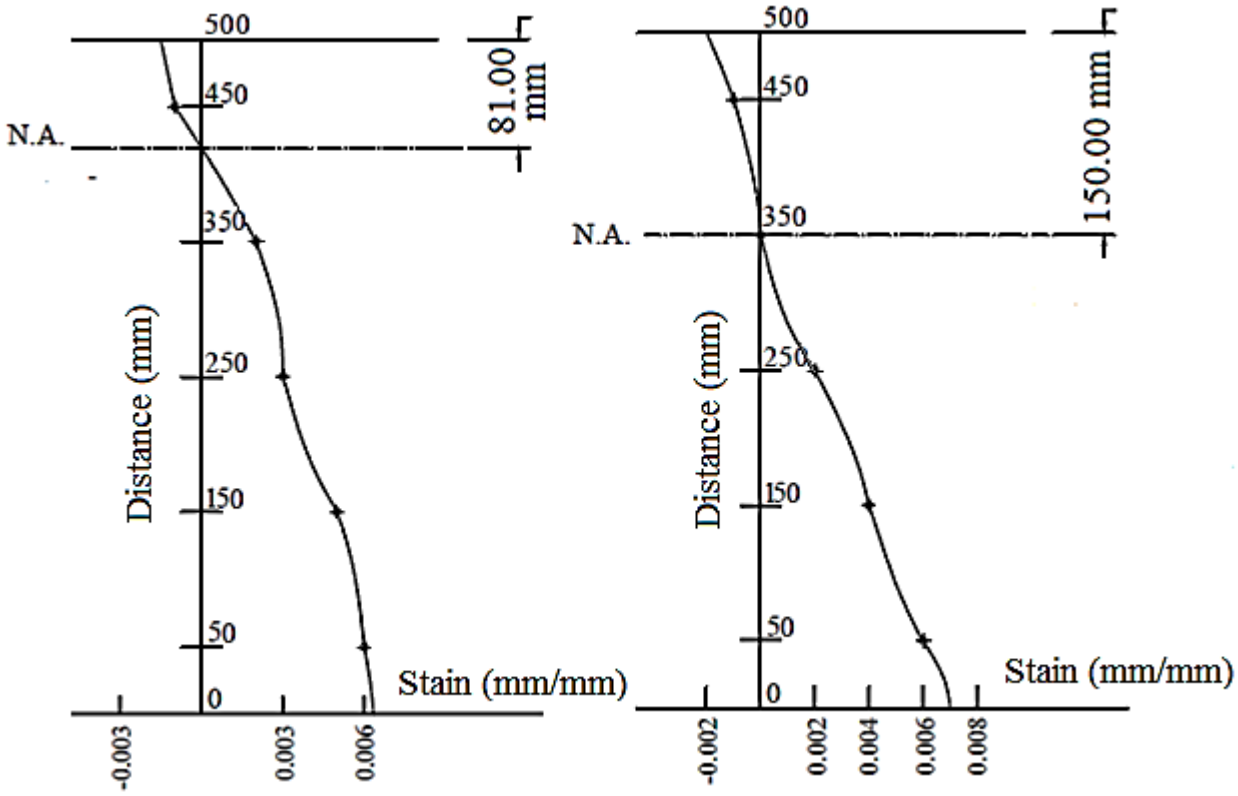

(b) Beam (C1). **(c) Beam (B2).**

Fig. 15. Typical concrete strain distribution profiles for some specimens.

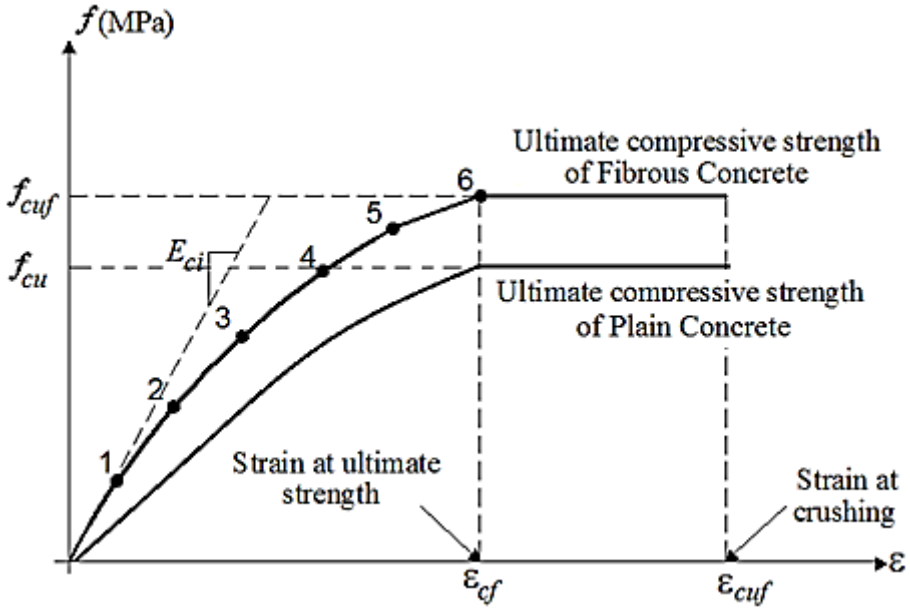

Fig. 16. Simplified compressive uniaxial stress- strain curve for concrete [10].

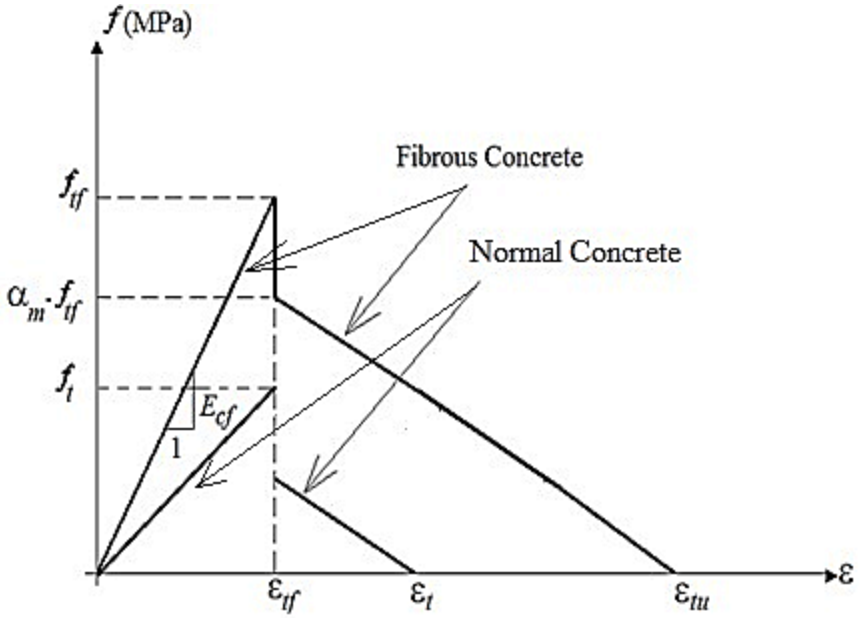

Fig. 17. Tension Stiffening Model [22].

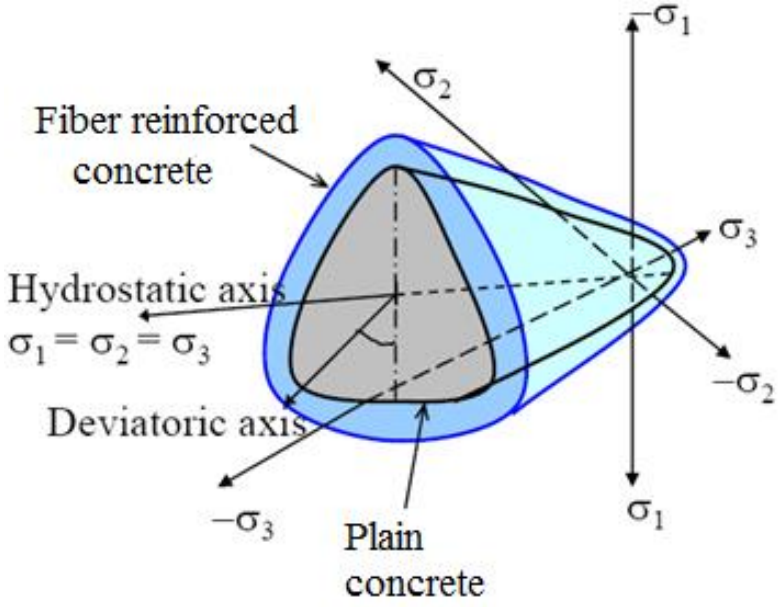

Fig. 18. The failure surface of fibre reinforced concrete [6].

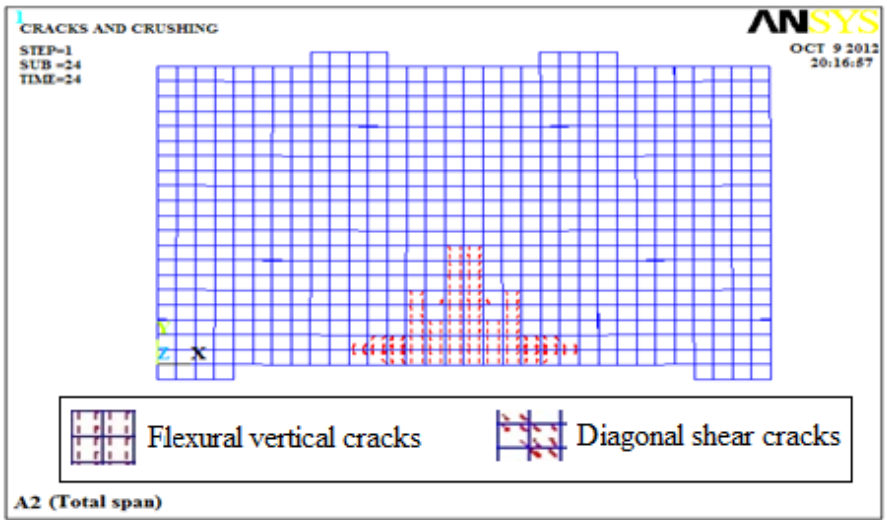

(a) At 30% of the failure load.

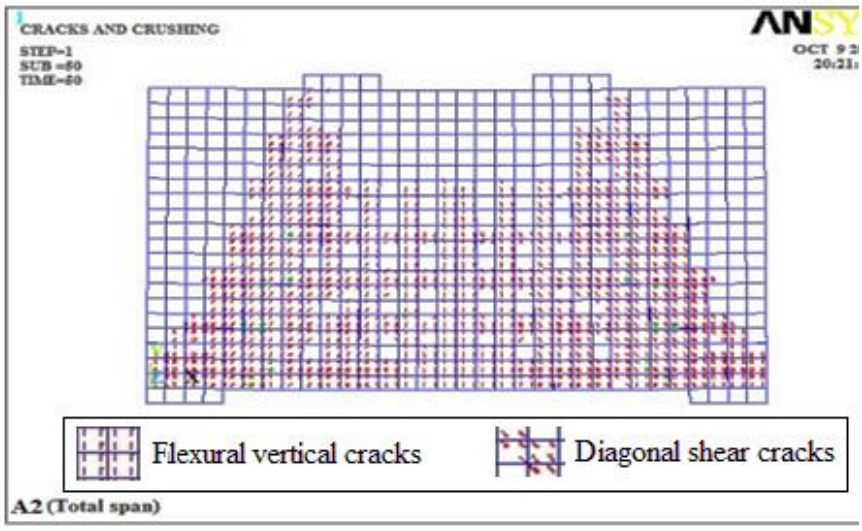

(b) At 50% of the failure load.

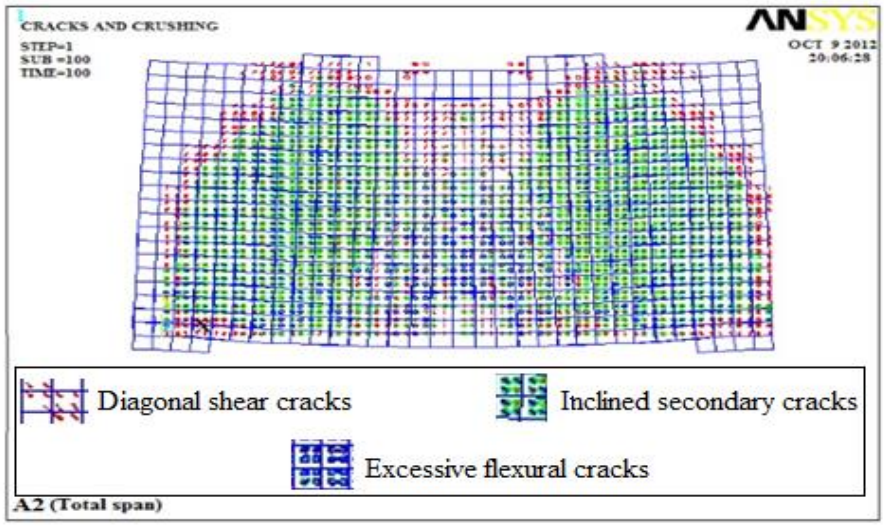

(c) At 90% of the failure load.

Fig. 19. Simulated crack propagation for the tested beam A2 [Shear-Compression failure (S.C)].

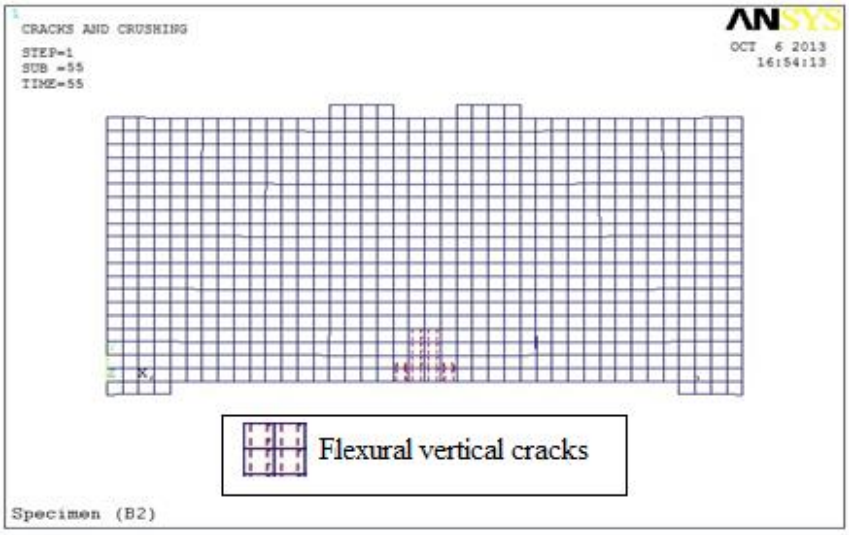

(a) At 25% of the failure load.

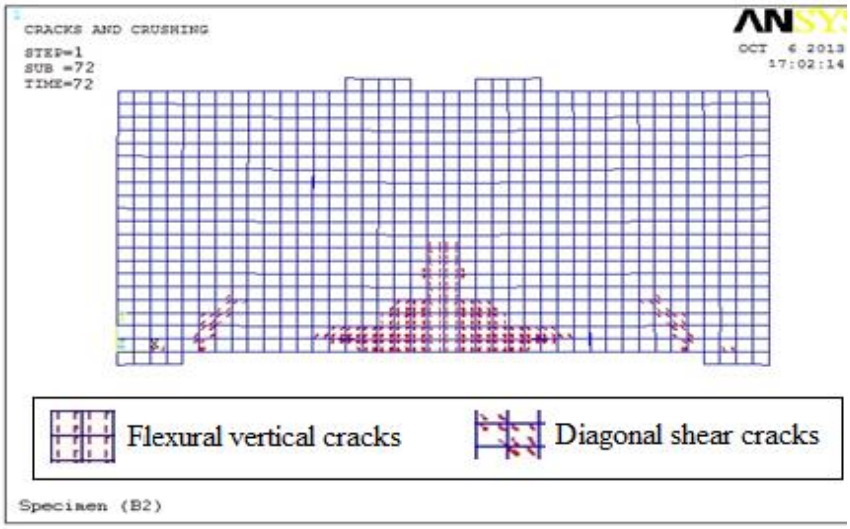

(b)At 50% of the failure load.

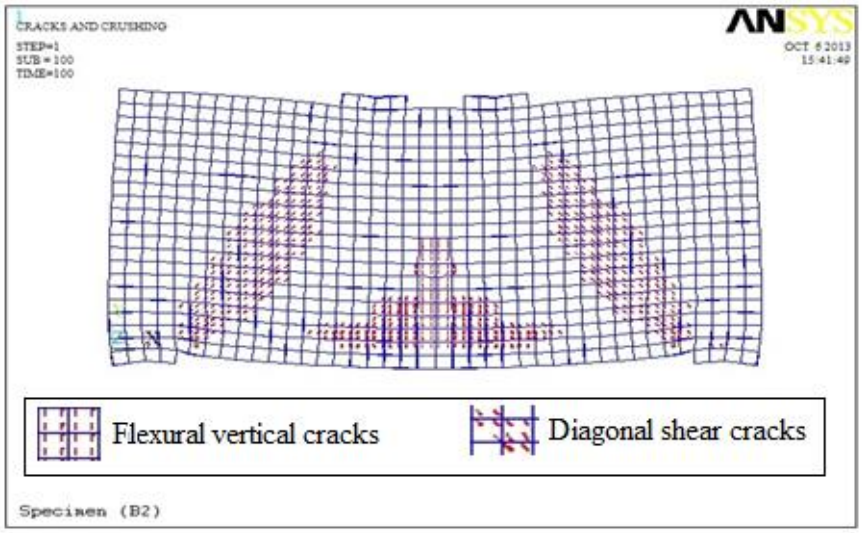

(c) At 90% of the failure load.

Fig. 20. Simulated crack propagation for the tested beam B2 [Diagonal-Splitting failure (D.S)].

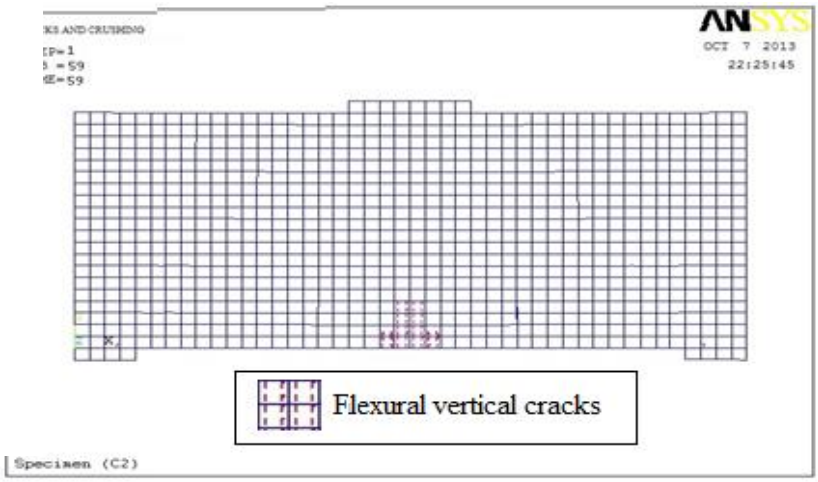

(a) At 25% of the failure load.

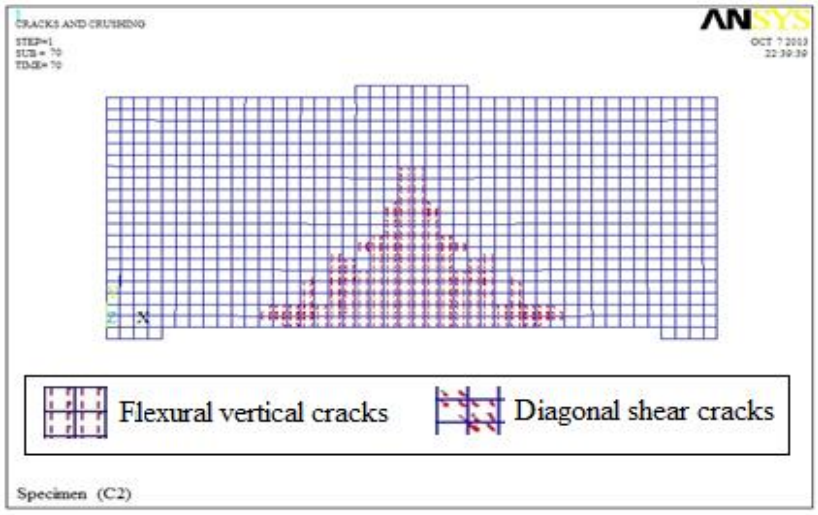

(b) At 50% of the failure load.

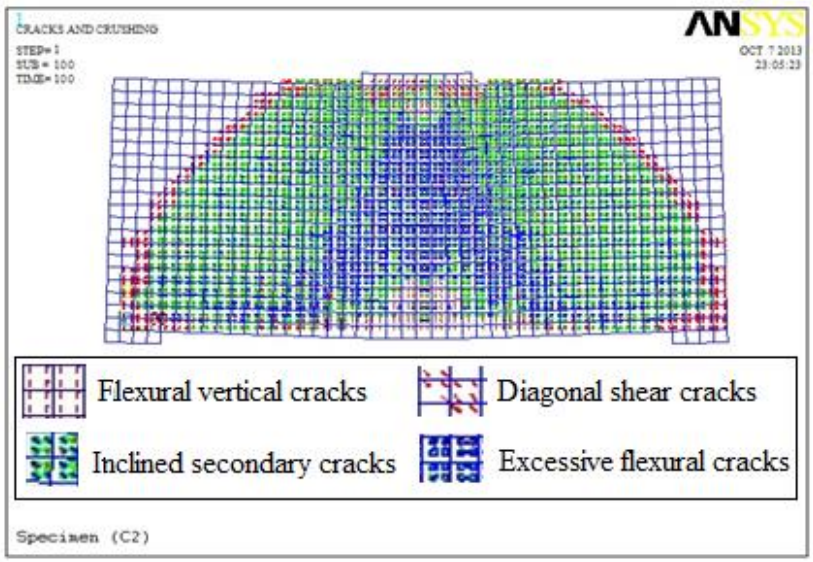

(c) At 90% of the failure load.

Fig. 21. Simulated crack propagation for the tested beam C2 [Crushing of concrete Strut (C.S)].

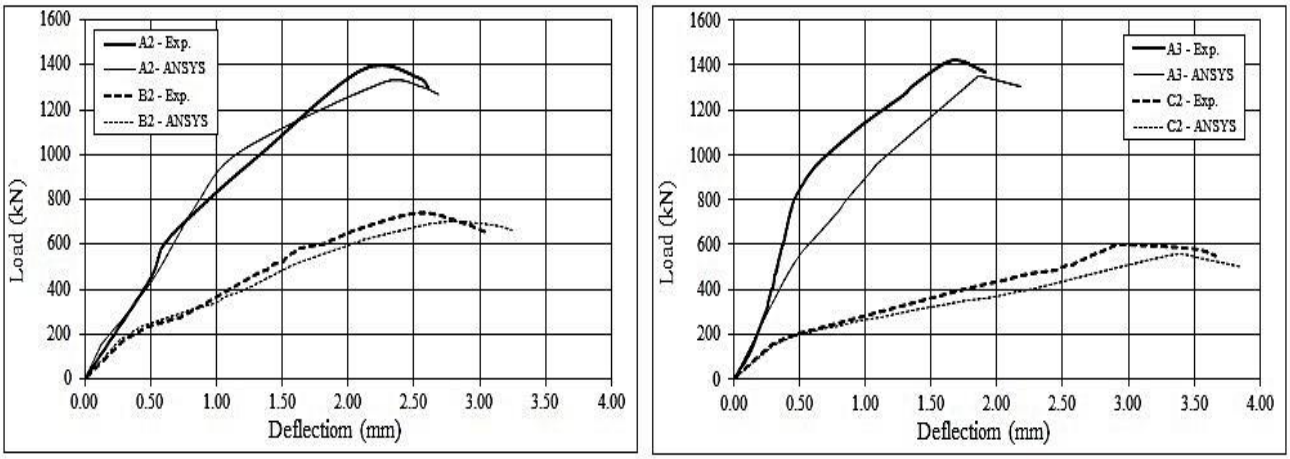

Fig. 22. ANSYS Vs experimental load-deflection curves.

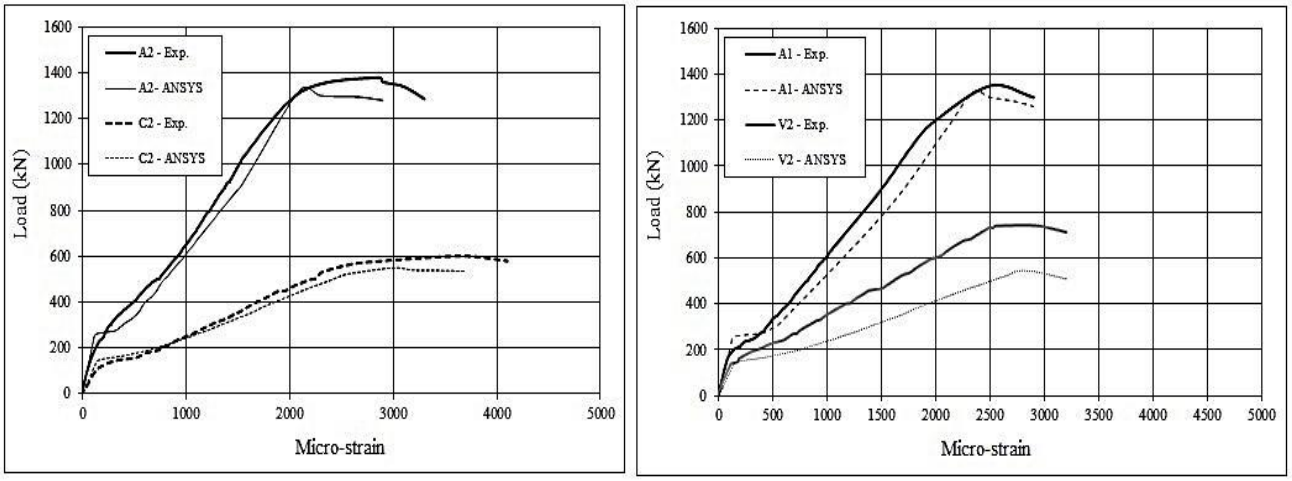

Fig. 23. ANSYS Vs experimental load-strain curves.

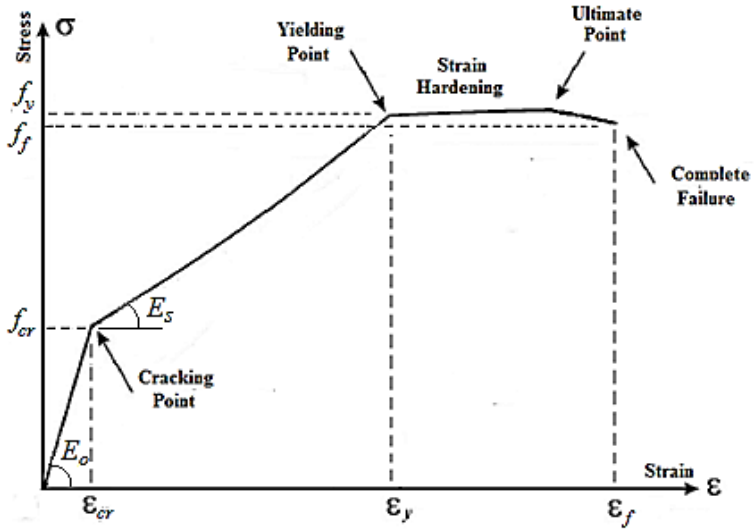

Fig. 24. Schematic stress-strain relationship for steel reinforcement.

REFERENCES

[1] CIRIA Guide 2, “The design of deep beams in reinforced concrete”, Ove Arup and Partners, Construction Industry Research and Information Association, London; 1977.

[2] ECP 203, "Egyptian code of practice for design and construction of reinforced concrete structures", Housing and Building Research Center, Ministry of Building and Construction. Giza, Egypt; 2017.

[3] ACI Committee 318M-11, “Building code requirements for structural concrete”, American Concrete Institute, Detroit, Michigan, Farmington Hills, USA; 2011: 189–190.

[4] Hong S. H. and Hong N. K., "Deformation capacity of structural concrete in disturbed regions", ACI Structural Journal; 2011; 108 (3): 267-276.

[5] Kong F. G., "Reinforced concrete deep beams", Second Edition, Taylor and Francis Group; 2003.

[6] Michael D. B., and Bayrak O., "Investigation of deep beams with various load configurations", ACI Structural Journal; 2007; 104(5): 611-620.

[7] Mihaylov B. I., Hunt B., Bentz E. C., and Collins M. P. "Three-parameter kinematic theory for shear behavior of continuous deep beams", ACI Structural Journal; 2015; 112(1): 47-58.

[8] Russo G., Venir R., and Pauletta M., "Reinforced concrete deep beams: shear strength model and design formula", ACI Structural Journal; 2005; 102(3): 429–437.

[9] Tang C. T. and Tan K. H., "Interactive mechanical model for shear strength of deep beams", ASCE Journal of Structural Engineering; 2004; 130 (10): 1534-1544.

[10] Beaudin J. J.,"Handbook of fibre reinforced concrete: principles, properties, developments and applications", Noyes Publications; 1990.

[11] Bentur A., and Sidney M., "Fibre reinforced cementitious composites", Second Edition, Elsevier Applied Science, London and New York; 1990.

[12] Williamson G. R., "The effect of steel fibres on the compressive strength concrete in fibre reinforced concrete", ACI Structural Journal, Detroit; 1974; SP (44): 95-207.

[13] Aguilar G., Matamoros A. B., Gustavo J. P. M., Ramírez J. A. and Wight J. K., "Experimental evaluation of design procedures for shear strength of deep reinforced concrete beams", ACI Structural Journal; 2002; 99(4): 539–548.

[14] Kwak Y., Eberhard M. O., Kim W., and Kim J., "Shear strength of steel fibre reinforced concrete beams without stirrups", ACI Structural Journal; 2002; 99(4): 530-538.

[15] Mansur M. A., and Ong K. C. G., "Behavior of reinforced fibre concrete deep beams in shear', ACI Structural Journal; 1991; 88(1): 98-105.

[16] Narayanan R., and Darwish I. Y. S., "Fibre concrete deep beams in shear", ACI Structural Journal; 1988; 85(S17): 141-149.

[17] Salamy M. R., Kobayashi H., and Unjoh S., "Experimental and analytical study on R.C deep beams", Asian Journal of Civil Engineering; 2005; 6(5):409-421.

[18] Wang F., Teng S., and Fan S.C., "Softened damage model for finite element analysis of structural concrete deep beams", ACI Structural Journal; 2001; 98(1): 27-35.

[19] Xu L.H. , Chi Y. , Li R. Y., and Jing Su, "Realization of ANSYS for nonlinear finite element analysis of steel fibre reinforced concrete deep beams, rock and soil mechanics", School of Civil and Architectural Engineering, Wuhan University, Wuhan, China, 2008.

[20] Ashour, S. A., Mahmood, K., and Wafa, F. F., "Influence of steel fibres and compression reinforcement on deflection of high strength concrete beams", ACI Structural Journal 1997; 94(6): 611-624.

[21] Naik, U. P., and Kute, S., "Effect of shear span to depth ratio on shear strength of steel fibre reinforced high strength concrete deep beam", Using ANN. International Journal of Advanced Structural Engineering; 2013; 29 (5): 1-12.

[22] Padmarajaiah, and Ramaswamy A., 'Behavior of fibre-reinforced prestressed and reinforced high-strength concrete beams subjected to shear", ACI Structural Journal; 2001; 98(5): 752-761.

[23] Yaseen, Z. M., Tran, M. T., Kim, S., Bakhshpoori, T., and Deo, R. C.," Shear strength prediction of steel fibers reinforced concrete beam using hybrid intelligence models: a new approach", Engineering Structures,2018, 177, 244-255.

[24] Zhang, Y., Liu, A., Chen, B., Zhang, J., Pi, Y. L., and Bradford, M. A., "Experimental and numerical study of shear connection in composite beams of steel and steel-fiber reinforced concrete", Engineering Structures, 2020,215, 110707.

[25] Hong, Z.J., Li, S. S., Xie, W., and Guo, Y. D., "Experimental study on shear capacity of high strength reinforcement concrete deep beams with small shear span–depth ratio", Journal of Materials, 13.5, 1218, 2020.

[26] Nguyen, H. T., Tan, K. H., and Kanda, T., "Effect of polypropylene and steel fibers on web-shear resistance of deep concrete hollow-core slabs", Engineering Structures, 2020, 210, 110273.

[27] Hayder K.H.H., Shakir, Q.M., and Al-Tameemi, H.A., "Behavior of high-strength self-consolidated reinforced concrete t-deep beams", The Open Construction and Building Technology Journal, 14.1 ,2020.

[28] Hong, Z.J., Li, S. S., Xie, W., and Guo, Y. D., "Experimental study on shear capacity of high strength reinforcement concrete deep beams with small shear span–depth ratio", Journal of Materials, 13.5, 1218, 2020.

[29] Gou, H., Zhu, H., Zhou, H., and Yang, Z., "Reinforcement mechanism of orientally distributed steel fibers on ultra-high-performance concrete", Construction and Building Materials, April 2021, Vol. 281, 122646.

[30] Zamri, N. F., Mohamed, R. N., and Elliott, K. S., "Shear capacity of precast half-joint beams with steel fibers reinforced self-compacting concrete", Construction and Building Materials, February 2021, Vol. 272, 121813.

[31] Abdul-Razzaq, K. S., Jalil, A. M., and Dawood, A. A.," Reinforcing struts and ties in concrete continuous deep beams", Engineering Structures, 2021,240, 112339.

[32] El-Barbary, A. A., "Performance of steel fibres reinforced concrete deep beams", Ph.D., Faculty of Engineering, Shoubra, Benha University, Cairo, Egypt; 2015.

[33] Abbass, A. , Abid, S., and Özakça, M., "Experimental investigation on the effect of steel fibres on the flexural behavior and ductility of high-strength concrete hollow beams", Advances in Civil Engineering; 2019, Article ID 8390345, 13 pages

[34] Lantsoght, E. O.L. ,"Database of shear experiments on steel fibre reinforced concrete beams without stirrups", February 2019 Online: (07:10:10 CET).

[35] Banthia, N., Fujikake, K, Kim, Y. H., and Gupta,R, "Fibre-reinforced cement composites: mechanical properties and structural implications", Doo-Yeol Yoo,2019.

[36] Gilbert, A.R.I, "Steel fibre-reinforced concrete beams—part II: strength, ductility and design", ACI Structural Journal 116 (2), December; 2018.

[37] ANSYS®, "Engineering analysis system user's manual", Theoretical Manual, Revision 10, ANSYS Inc., South Pointe Technology Drive, FLEXlm License Manager Canonsburg, PA; 2009.

[38] Hsu, L. S., and Hsu, C. T., "Stress-strain behavior of steel fibre high strength concrete under compression", ACI Structural Journal; 1994; 91(4): 448-457.

[39] Soroushian P., and Lee C. D., "Constitutive modeling of steel fibre reinforced concrete under direct tension and compression", Proceeding of the International Conference on Recent Developments in Fibre Reinforced Cements and Concrete, Cardiff, U.K.; 1989: 363-377.

[40] Lihua X., Yin C., Jie S., and Dongtao X., "Nonlinear finite element analysis of steel fibre reinforced concrete deep beams", Wuhan University, Journal of Natural Science; 2008; 13(2): 201-206.

[41] Chern J. C., Yang J. H., and Chen H. W., "Behavior of steel fibre reinforced concrete in multiaxial loading", ACI Material Journal;1992; 89(1): 32-40.

[42] William, K. J., and Warnke, E. D., "Constitutive model for the triaxial behavior of concrete", Proceeding of the International, Association for Bridge and Structural Engineering, ISMES, Bergamo, Vol. 19; 1975, pp.174.

[43] Al-Quraishy A.Q., "Behavior of Normal, High and Ultra-High Strength Concrete in Direct Shear", International Journal of Civil Engineering and Technology, 9(2), 2018, pp. 349-360.